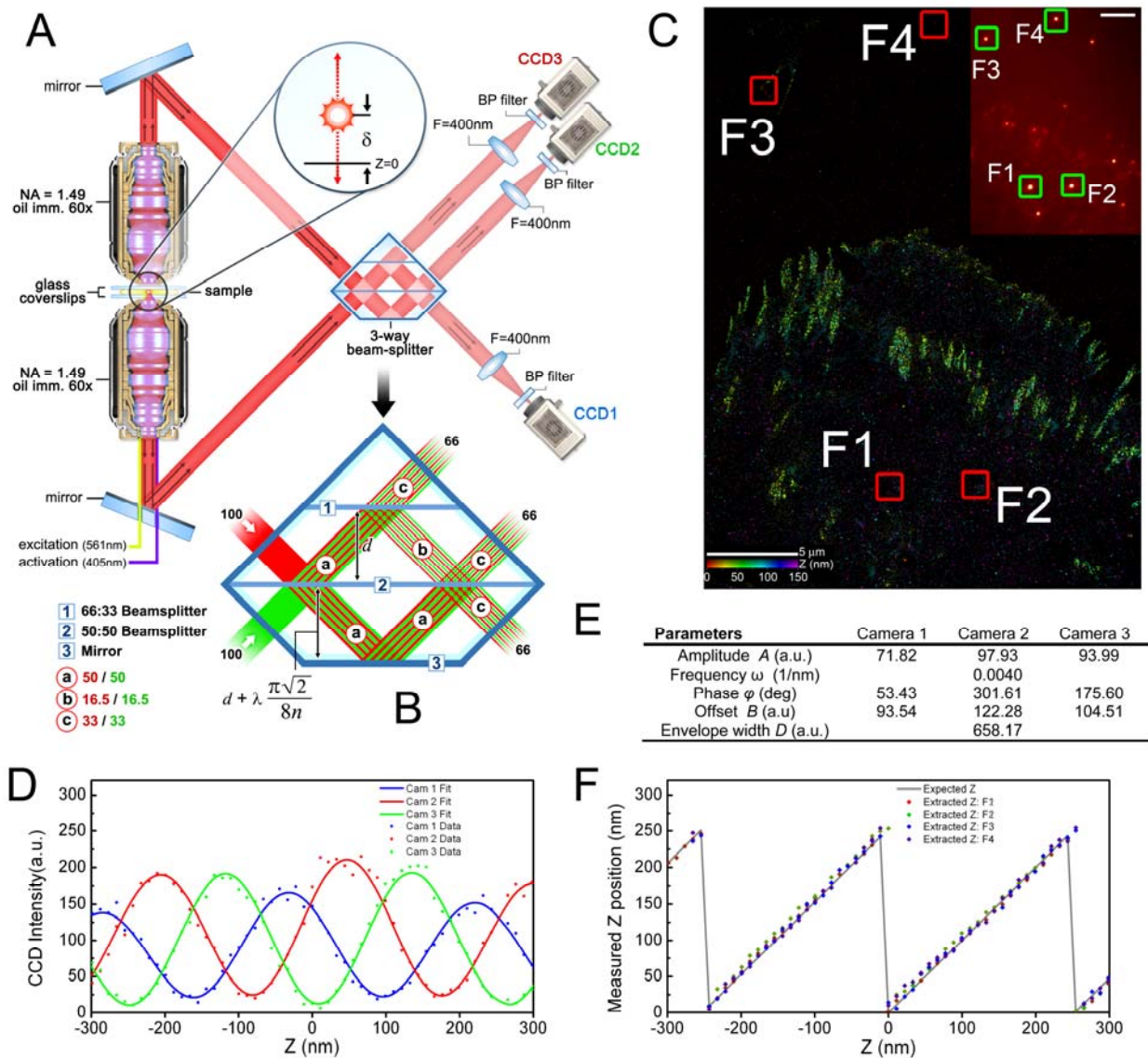


Supplementary Figures 1-22

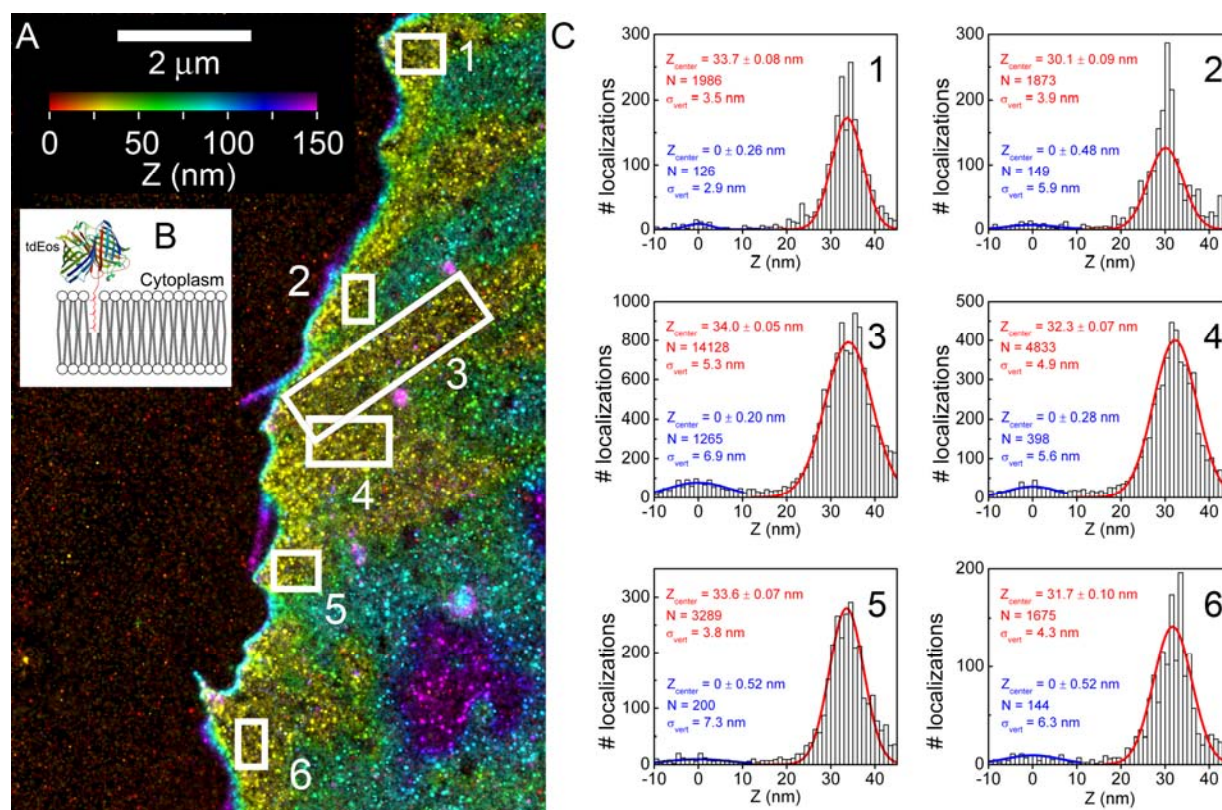
Supplementary Figure 1. Schematics of iPALM

(A) Optical configuration of the iPALM system. Fluorescence emission is collected by two opposed objective lenses. Each emitted photon travels through both beams, whose pathlength difference is directly proportional to the z-coordinate, and gives rise to a phase difference when recombined in **(B) 3-way beamsplitter**, custom-designed to project 3 beams with $2\pi/3$ phase difference between one another. Each of the 3 interfered beams is detected by an EMCCD camera. **(C-F) Example of iPALM calibration:** (C), iPALM image of U2OS cell expressing vinculin-tdEos, color encoded z coordinate relative to substrate surface. Cells are plated on coverglass with gold nanoparticles sparsely immobilized (e.g. F1-F4) to serve as fiducials. (C, inset) summed raw CCD images for the calibration data, with fiducials highlighted (green boxes). Red boxes in iPALM image indicated corresponding fiducials positions (not rendered). (D), the intensities of fiducial F1 in 3 cameras as a function of sample z position scanned by a piezoelectric sample holder, fit parameters shown in (E). (F), extracted z position of fiducials F1-F4 (diamonds) based on parameters in (E) versus expected values (solid line).



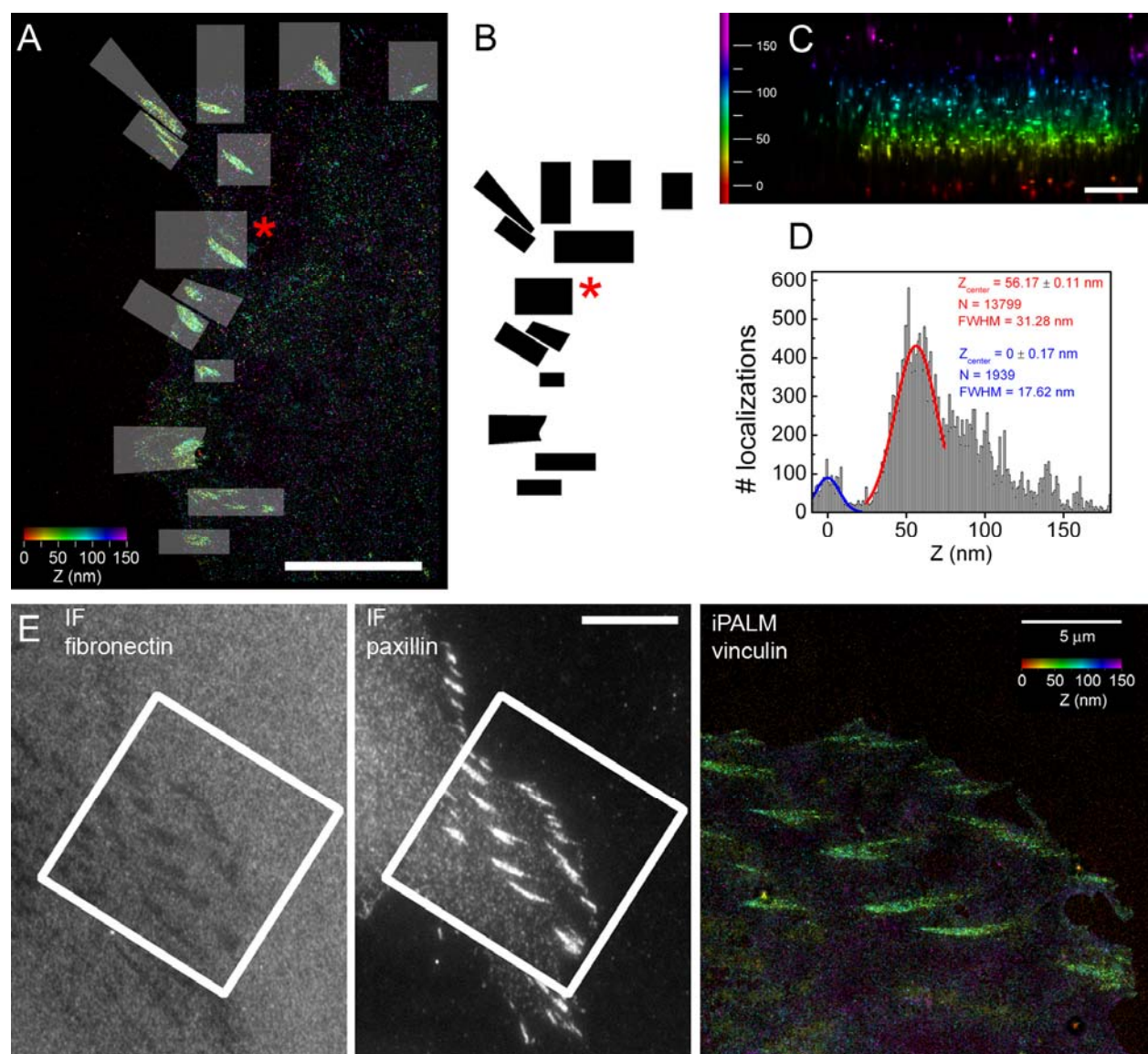
Supplementary Figure 2. Validation of vertical resolution from imaging a plasma-membrane associated PA-FP marker

(A) iPALM top view of the U2OS cell expressing CAAX-tdEos marking the inner plasma membrane from Fig. 1a, with the FA areas highlighted (box 1-6). The ventral plasma membrane is seen consisting of flat yellow areas corresponding to FA. The color gradient reflects the contour of the plasma membrane relative to the substrate. **(B)** Schematic diagram for CAAX-tdEos localization to the cytoplasmic leaflet of the plasma membrane. **(C)** Histogram (1-nm bins) of the vertical (Z) coordinates for areas 1-6. Gaussian fits and fit parameters are shown for CAAX-tdEos (red) and substrate (blue). The substrate peak for each area is set to $z = 0$ nm. The plasma membrane under FAs (boxed areas) appears to be very flat, with width parameter σ_{vert} of 4-5 nm (corresponding to full-width-half-maximum of ~ 10 nm), as seen in (C), demonstrating both the membrane flatness in FA regions and iPALM spatial resolution.



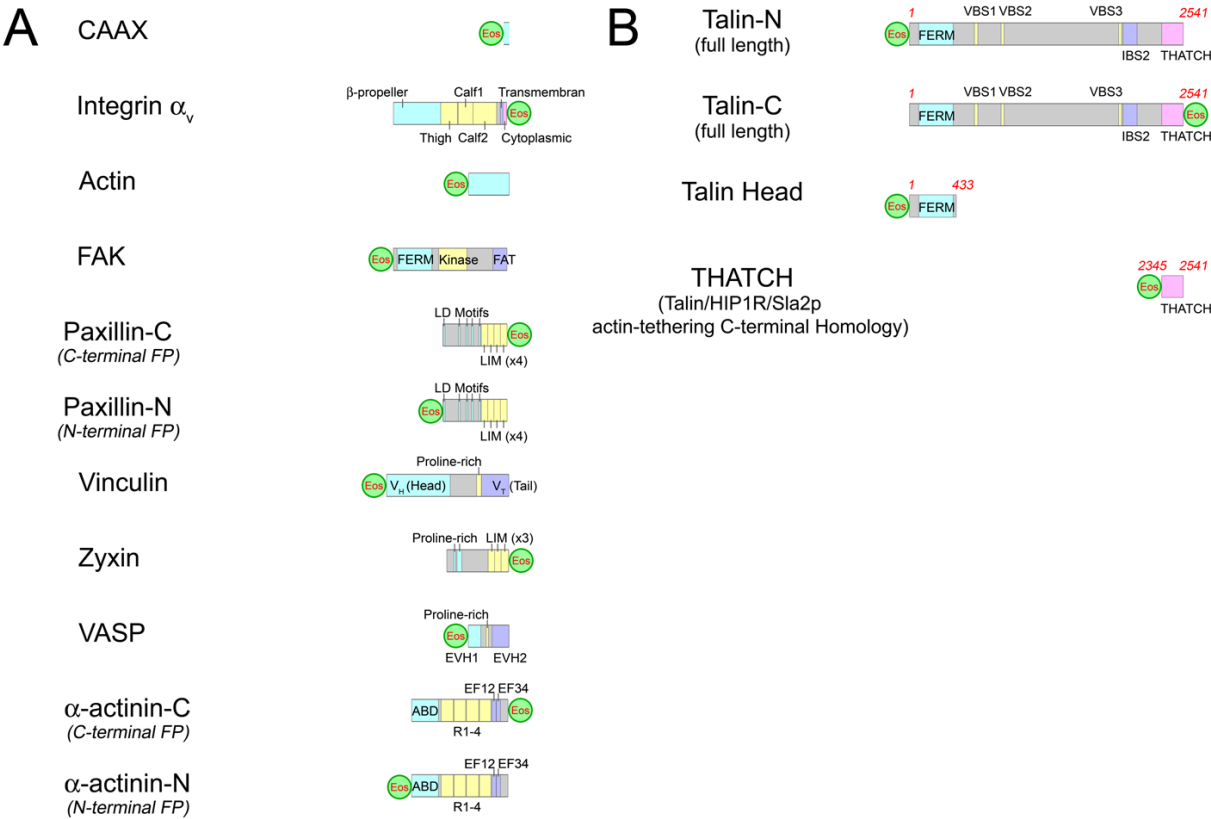
Supplementary Figure 3. Analysis of FA protein distribution

(A) iPALM image of tdEos-vinculin in a U2OS cell (same cell as in Fig. 2e-f) with ROI (gray overlays) and binary mask **(B)** for the FAs and the surrounding region used to calculate substrate vertical position. Scale bar, 10 μm . **(C)** Sideview (xz) projection of the FA marked in A (asterisk). Cell edge is to the left. Horizontal scale bar, 500 nm. Vertical (z) scale indicated by color. **(D)** Histogram of the Z coordinates (1-nm bins) for molecules in the FA area highlighted by an asterisk in A&B. Gaussian fits and fit parameters for the vinculin (red) and substrate (blue) peaks are shown. **(E)** Comparison of iPALM image of tdEos-vinculin (right) and conventional immunofluorescence (IF) micrograph of paxillin and fibronectin (left, center) taken afterward (Supplementary Note 2). Boxes correspond to area imaged by iPALM. Scale bars, 5 μm for iPALM, 10 μm for IF. Uniform staining for fibronectin is observed on coverglasses with areas corresponding to FA showing lower fibronectin staining due to the binding of fibronectin epitopes and steric exclusion of antibodies by integrin ECM receptors³⁶.



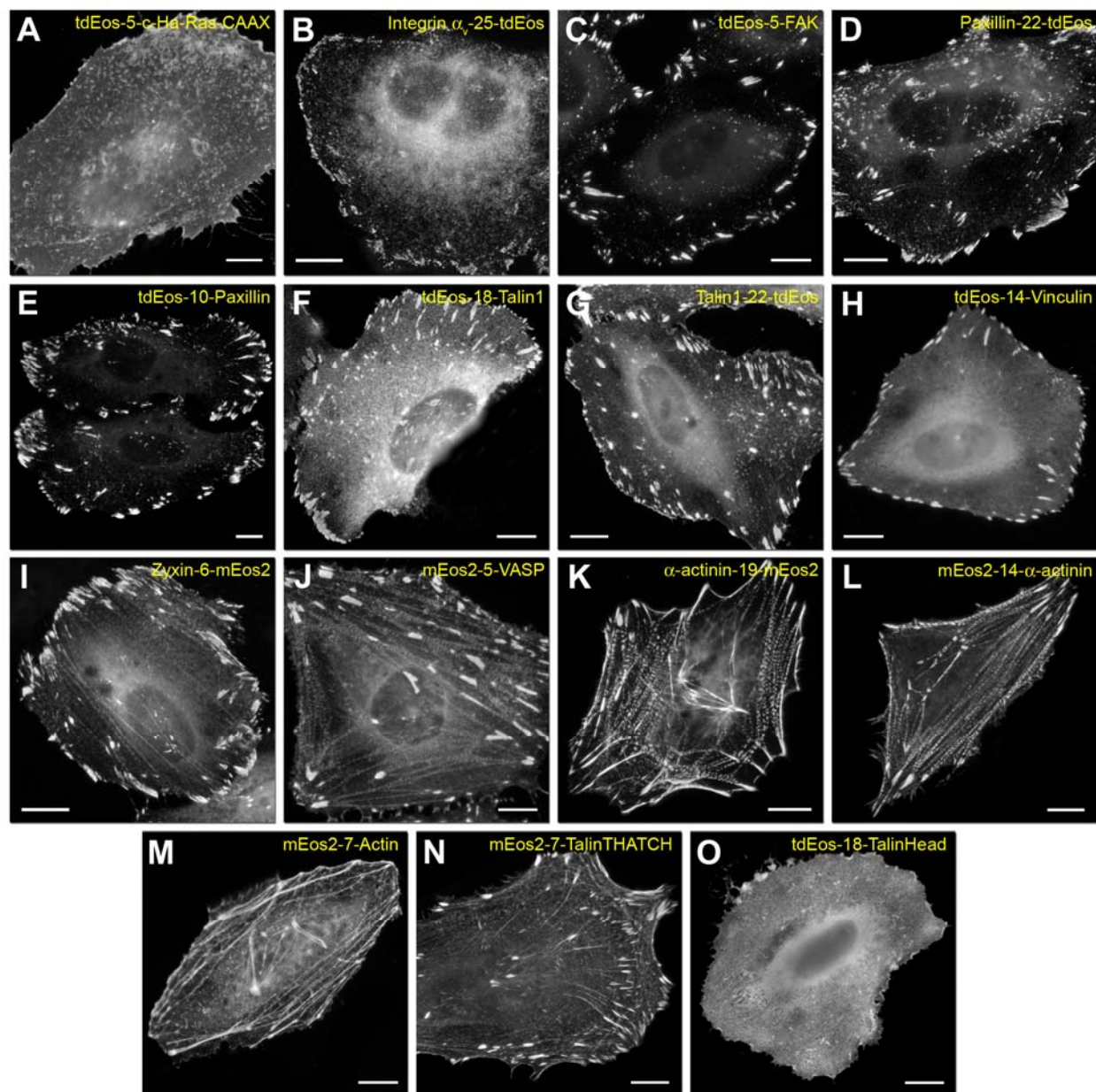
Supplementary Figure 4. PA-FP fusion protein expression constructs

Schematic diagram of FA protein PA-FP fusion expression constructs, drawn to scale with the sequence length in residues. **(A)** FA component constructs imaged in Fig. 1-2 and corresponding Supplementary figures. **(B)** Talin expression constructs imaged in Fig. 3 and corresponding Supplementary figures, with important domains noted, and amino acid numbers indicated.



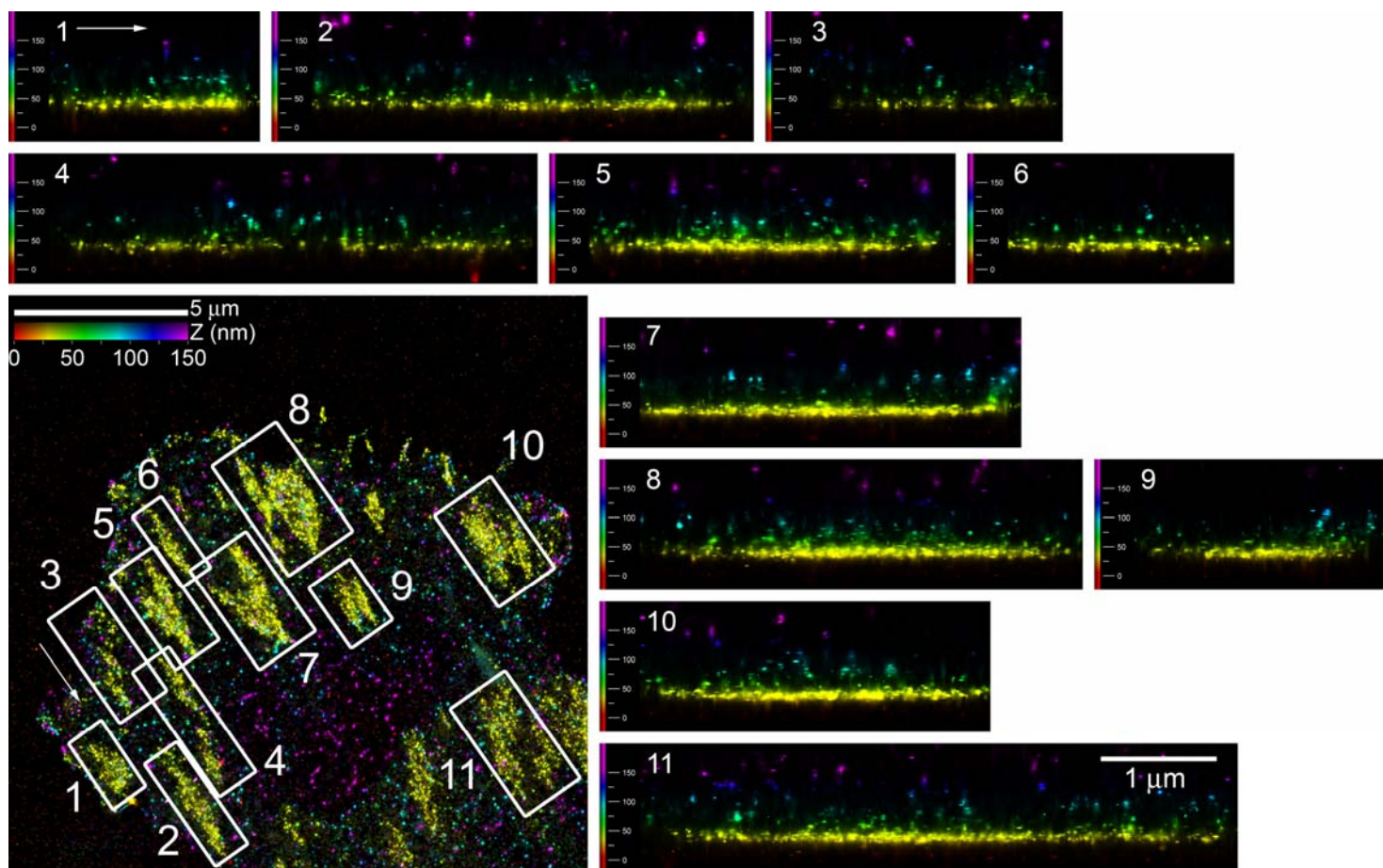
Supplementary Figure 5. Localization of PA-FP fusion protein expression constructs

Fluorescence micrographs (green fluorescence channel for non-photoconverted EosFP) of HeLa Cells expressing fusion constructs. Protein names indicate the PA-FP used and linker lengths (e.g. tdEos-10-paxillin: paxillin conjugated at N-terminus with tdEos via 10 amino acid linker). **(A)** tdEos-5-[c-Ha-Ras CAAX]; **(B)** Integrin α_v -25-tdEos; **(C)** tdEos-5-FAK; **(D)** Paxillin-22-tdEos (Paxillin-C); **(E)** tdEos-10-Paxillin (Paxillin-N); **(F)** tdEos-18-Talin1 (Talin-N); **(G)** Talin1-22-tdEos (Talin-C); **(H)** tdEos-14-Vinculin; **(I)** Zyxin-6-mEos2; **(J)** mEos2-5-VASP; **(K)** α -actinin-19-mEos2 (α -actinin-C); **(L)** mEos2-14- α -actinin (α -actinin-N); **(M)** mEos2-7-Actin; **(N)** mEos2-7-TalinTHATCH; **(O)** tdEos-18-TalinHead. Scale bars, 10 μ m.



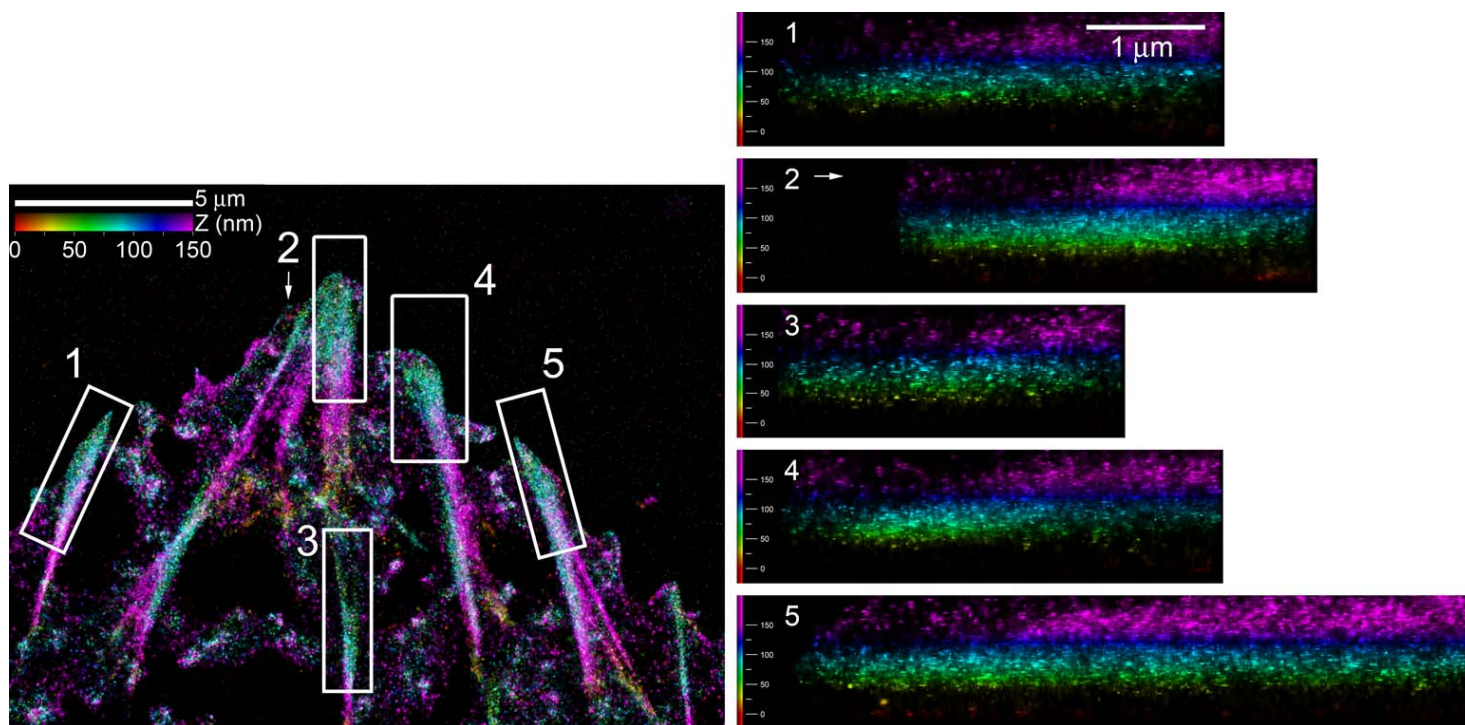
Supplementary Figure 6. Integrin α_v

Topview iPALM image (**left**) of Integrin α_v -tdEos in U2OS cell. Sideview projections are shown for boxed areas (**1-11**), same color scale as topview. Z coordinates relative to substrate surface (0-150 nm) indicated by color bar (left) and vertical scale (sideviews). Arrows indicate sideview orientation. All sideviews are on the same scale (scale bar, 1 μm). Area 7 corresponds to Fig. 1e. Integrin α_v -tdEos localized to a narrow plane at $z \sim 30$ -35 nm from the substrate surface.



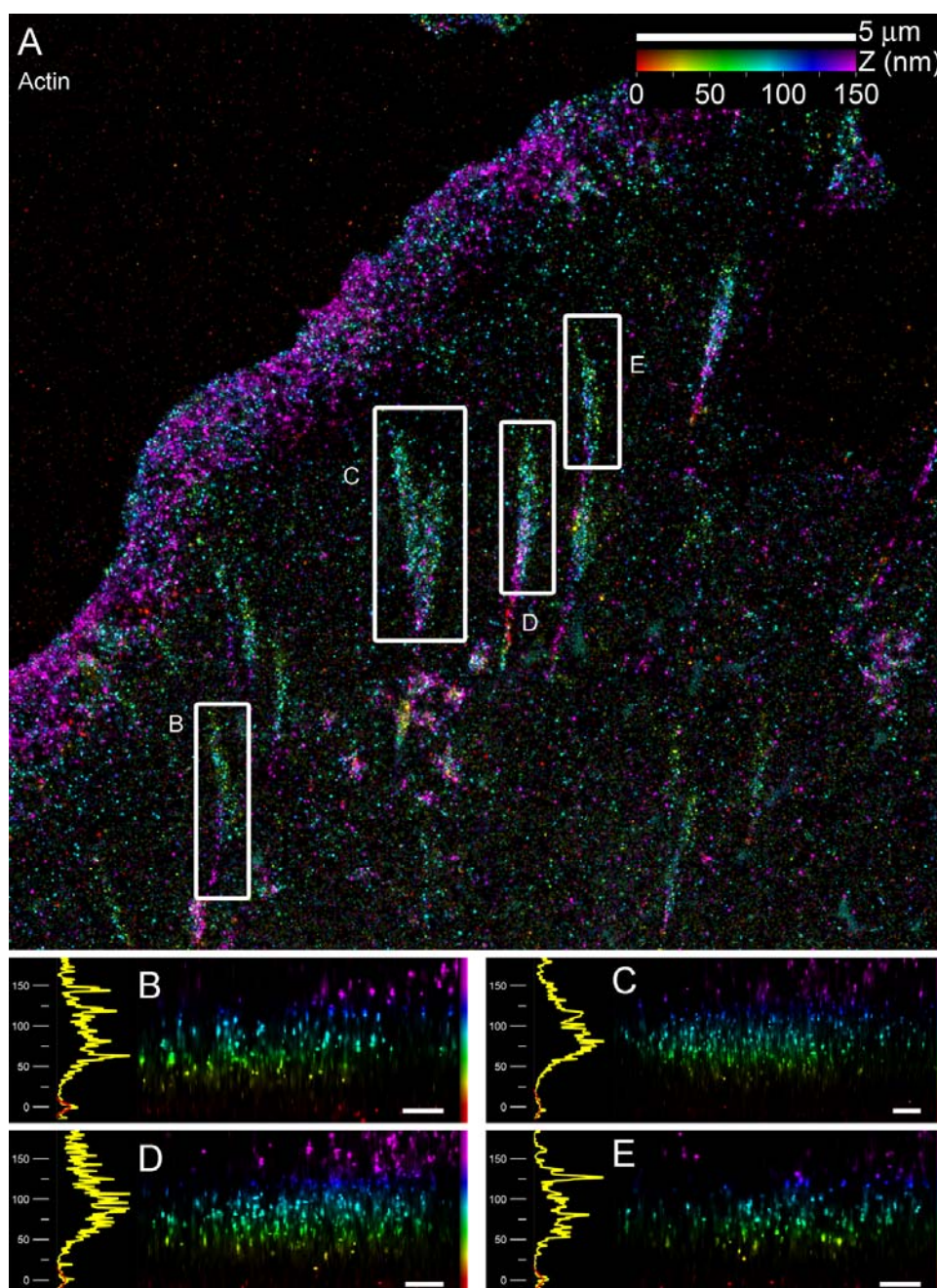
Supplementary Figure 7. Actin

Topview iPALM image (**left**) of Actin-mEos2 in U2OS cell. Sideview projections (**right**) are shown for boxed areas (**1-5**), same color scale as topview. Z coordinates relative to substrate surface (0-150 nm) indicated by color bar (left) and vertical scale (sideviews). Arrows indicate sideview orientation. All sideviews are on the same scale (scale bar, 1 μm). Area 2 corresponds to Fig. 1g. Actin-mEos2 localizations are largely excluded below $z \sim 50$ -60 nm, but extend upward into the cell interior.



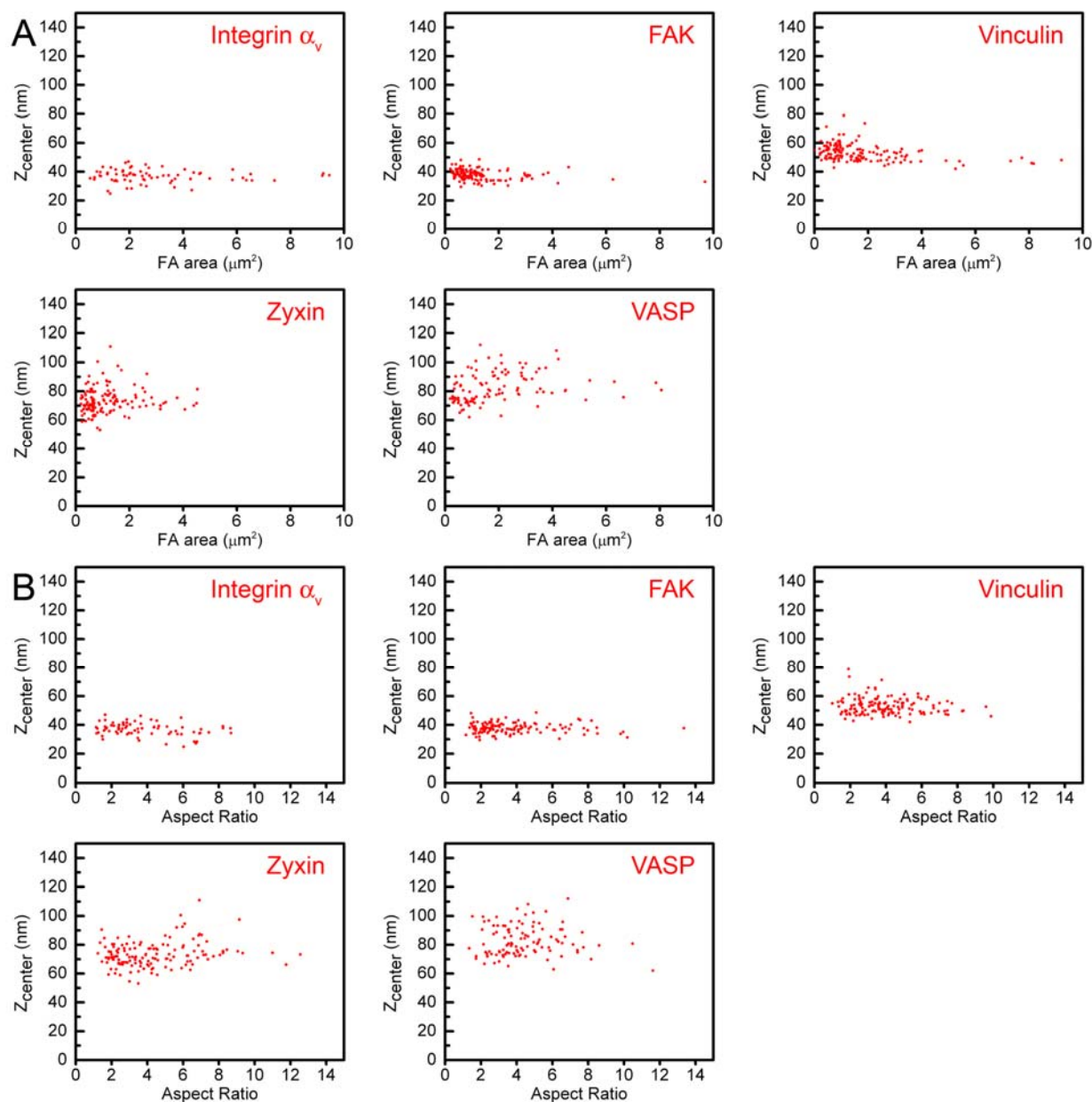
Supplementary Figure 8. Actin

Topview iPALM image **(A)** of Actin-mEos2 in a U2OS cell that also displays lamellipodial actin networks. Sideview projections and histograms **(B-E)** are shown for boxed areas, same color scale as A. Z coordinates relative to substrate surface (0-150 nm) indicated by color bar (A) or color and vertical scale bar (B-E). Sideviews are oriented with the nearest cell edge (top edge in A) to the left. Scale bars, 500 nm (B-E). Actin localizations are largely excluded below $z \sim 50$ -60 nm. Actin localizations also extend continuously with stress fibers upward into the cell beyond the imaging range. Lamellipodial actin networks seen at the cell edge are localized at $z > 100$ nm. Note that since the actin networks contain both the unlabeled endogenous actin and expressed actin-mEos2 probes, the actin localizations are not dense enough to distinguish individual f-actin filaments.



Supplementary Figure 9. Vertical positions of FA proteins as a function of FA size and morphologies

Plot of z_{center} protein positions (nm) as a function of FA area (μm^2) (A) or aspect ratio (ratio of major to minor axes of best-fit ellipse) (B). Each point in A & B represents an FA region. (C) Correlation coefficients of z_{center} with area (R_{area}), aspect ratio (R_{aspect}), and major and minor axes of best-fit ellipse (R_{major} and R_{minor}).

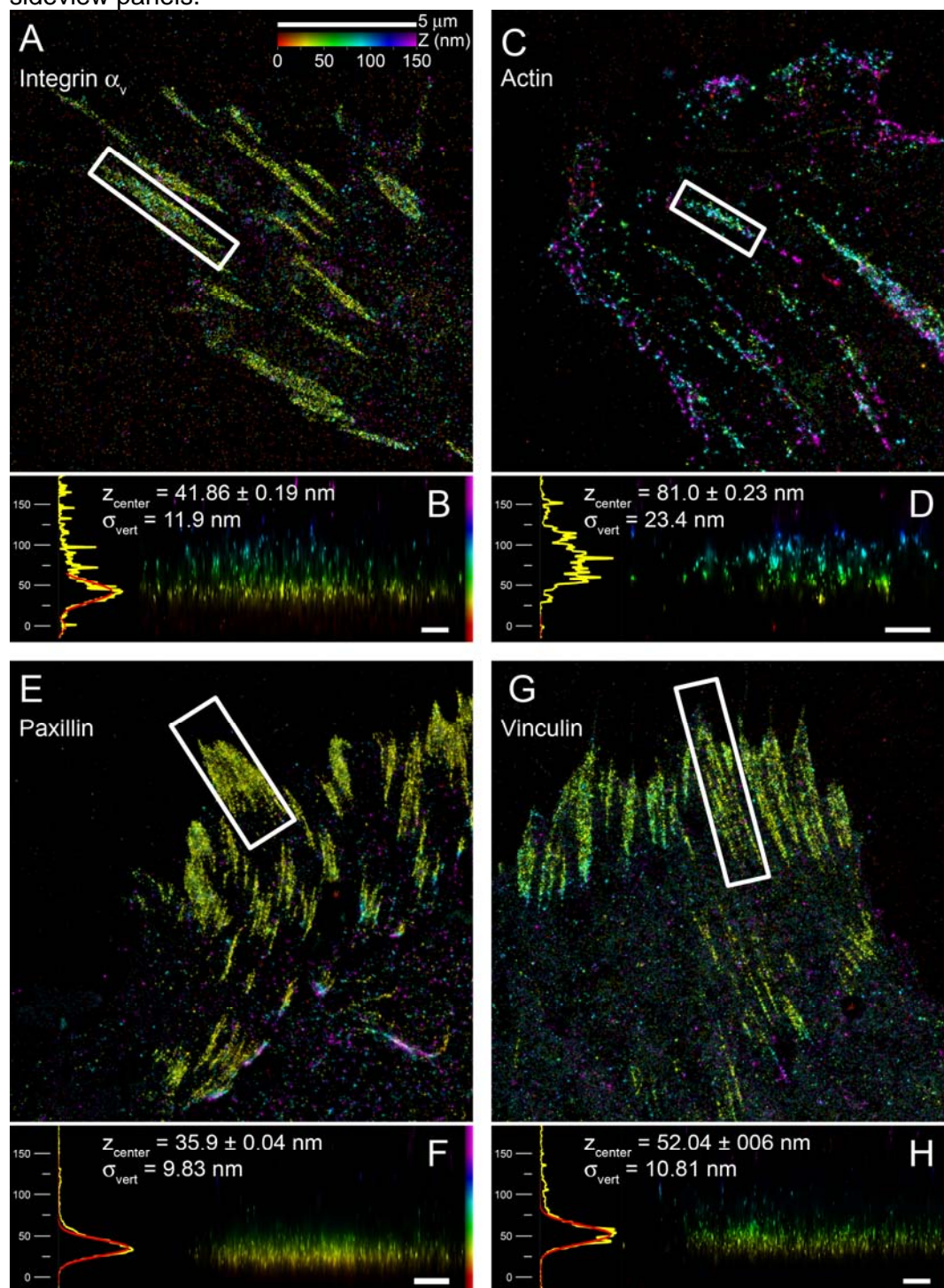


Supplementary Figure 9 (continued)

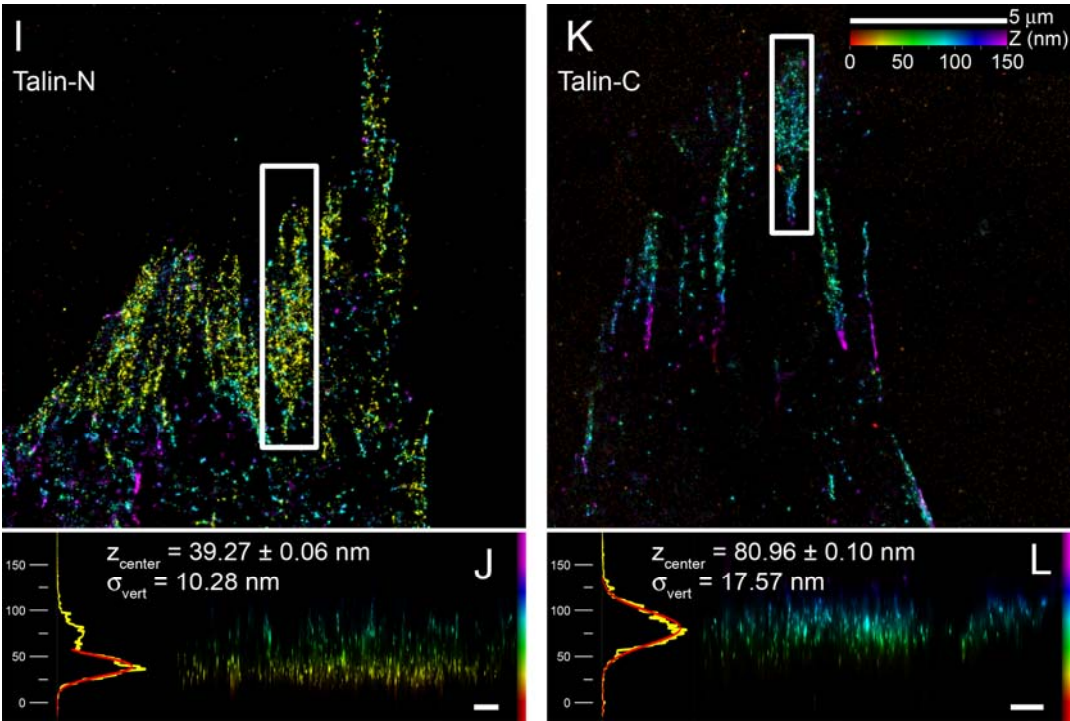
C

FA component	R _{area}	R _{aspect}	R _{major}	R _{minor}
Integrin α_v	-0.0313	-0.2838	-0.1694	0.0704
FAK	-0.1409	-0.0234	-0.0830	-0.1524
Paxillin-C	-0.0992	-0.0502	-0.1011	-0.0287
Paxillin-N	-0.1614	-0.0516	-0.1059	-0.0884
Vinculin	-0.3708	-0.1213	-0.3170	-0.2453
Zyxin	0.1018	0.2132	0.2202	0.0356
Talin-N	-0.1740	-0.0739	-0.0911	-0.0016
Talin-C	0.0978	0.1647	0.1402	-0.0024
VASP	0.2794	0.0852	0.2393	0.2105
α -actinin-C	0.0128	0.1276	0.1116	0.0006
α -actinin-N	0.0578	0.1483	0.1226	-0.0778

Supplementary Figure 10. FA protein localizations in Mouse Embryonic Fibroblasts (MEF) Topview iPALM images of MEF cells expressing PA-FP fusion constructs, sideview projection images of highlighted FAs, histograms of vertical distributions (1-nm bins), and z_{center} and σ_{vert} parameters for the distribution of Integrin α_v -tdEos (**A&B**), Actin-mEos2 (**C&D**), Paxillin-C-tdEos (**E&F**), Vinculin-tdEos (**G&H**), Talin-N-tdEos (**I&J**), and Talin-C-tdEos (**K&L**). FA protein localizations similar to those in U2OS cells are observed. Scale bars, 500 nm for all sideview panels.

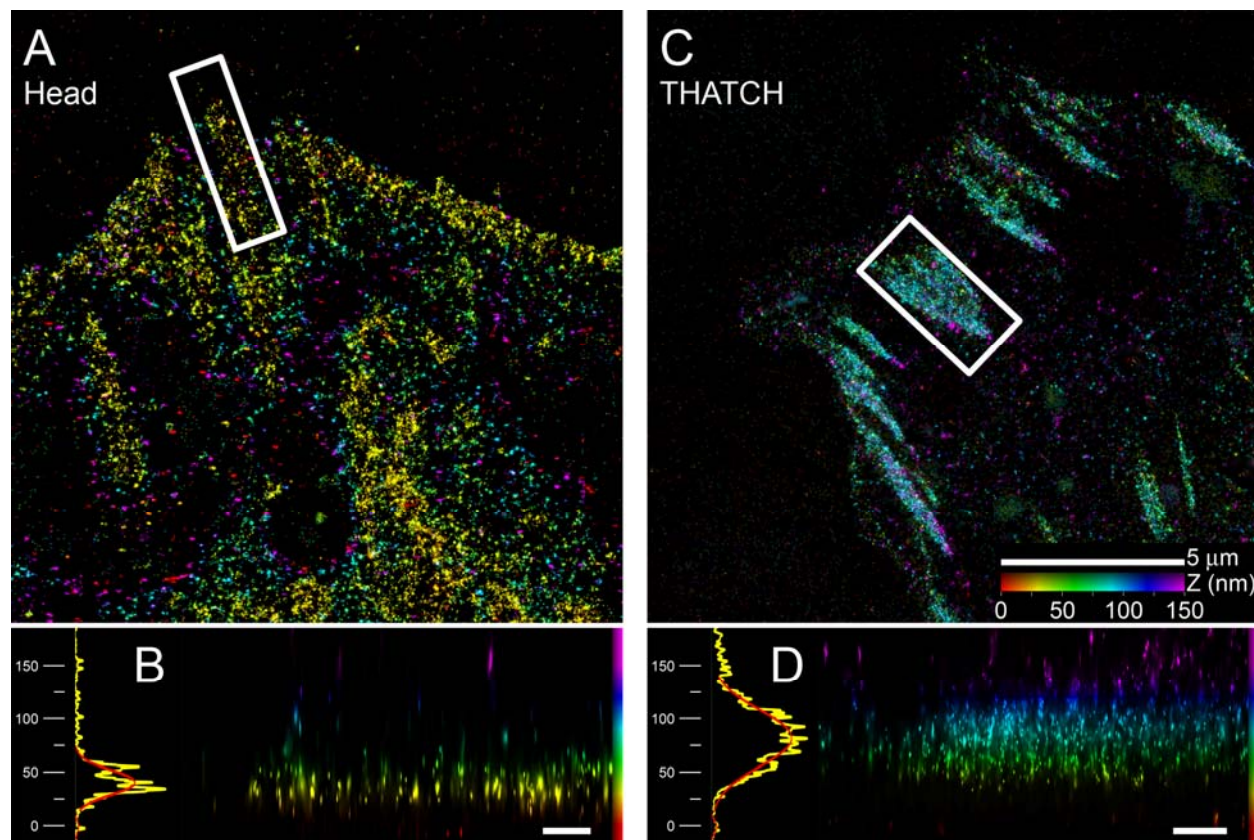


Supplementary Figure 10 (continued)



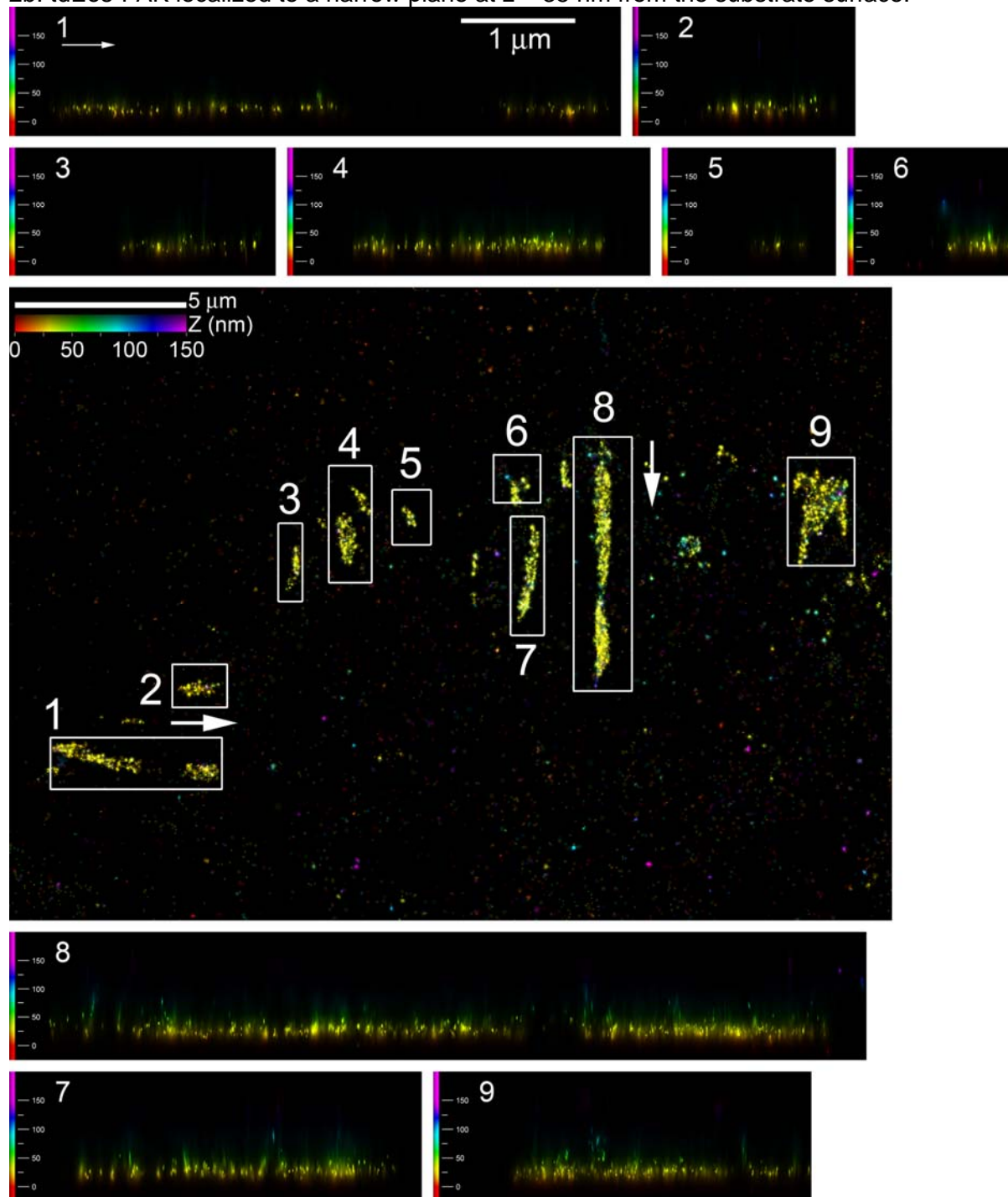
Supplementary Figure 11. Localizations of Talin head and tail fragments

Topview iPALM images, sideview projections, and histograms (1-nm bins) of vertical localizations for highlighted FAs, of U2OS cells expressing PA-FP fusion constructs of talin head fragment (FERM domain) (**A&B**), and talin tail fragment (THATCH domain) (**C&D**). Talin head domain appears to localize close to the plasma membrane, while the vertical position of THATCH domain appears to coincide with Talin-C and actin localizations. Scale bars, 500 nm (B, D).



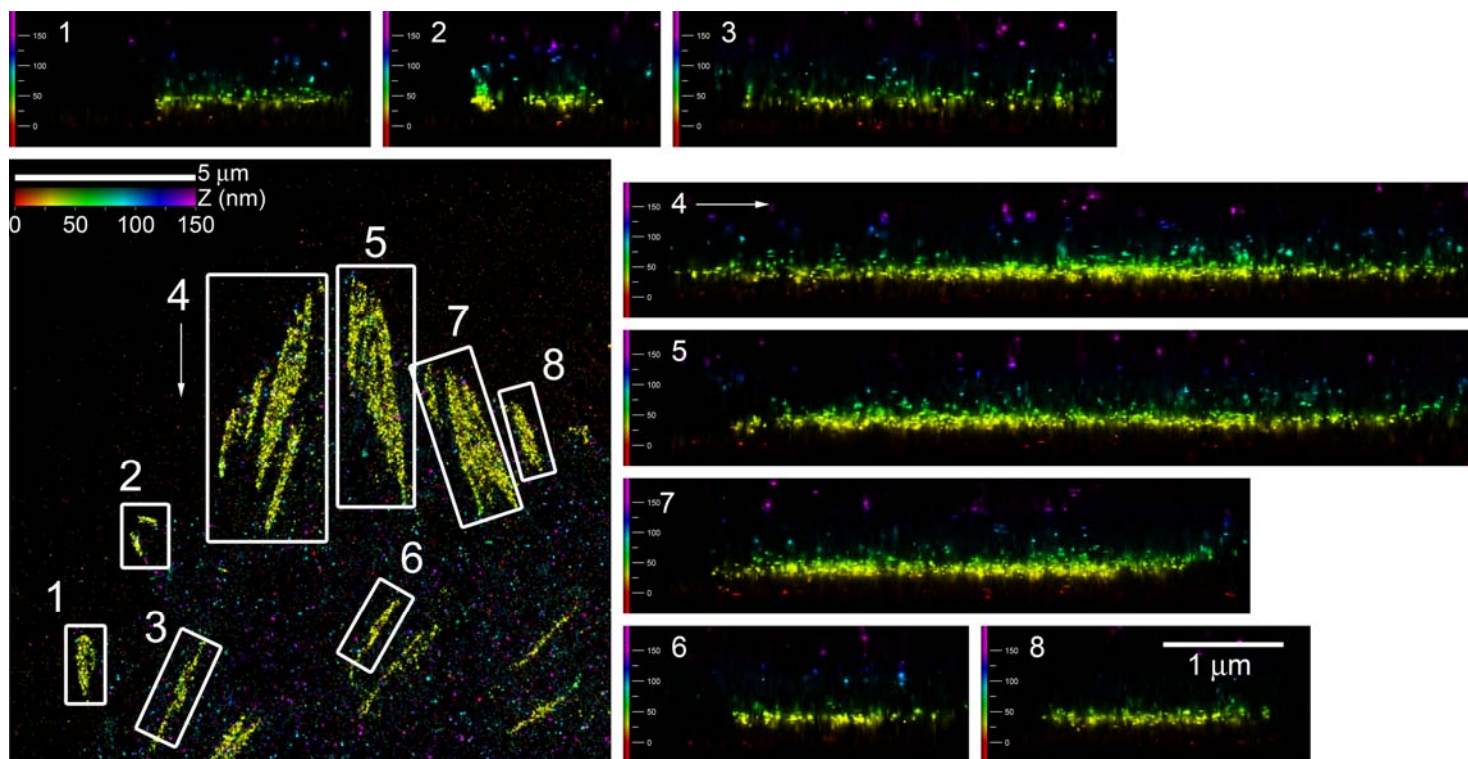
Supplementary Figure 12. Focal Adhesion Kinase (FAK)

Topview iPALM image (**center**) of tdEos-FAK in U2OS cell. Sideview projections are shown for boxed areas (**1-9**), same color scale as topview. Z coordinates relative to substrate surface (0-150 nm) indicated by color bar (center) and vertical scale (sideviews). Arrows indicate sideview orientation. All sideviews are on the same scale (scale bar, 1 μm). Area 8 corresponds to Fig. 2b. tdEos-FAK localized to a narrow plane at $z \sim 35$ nm from the substrate surface.



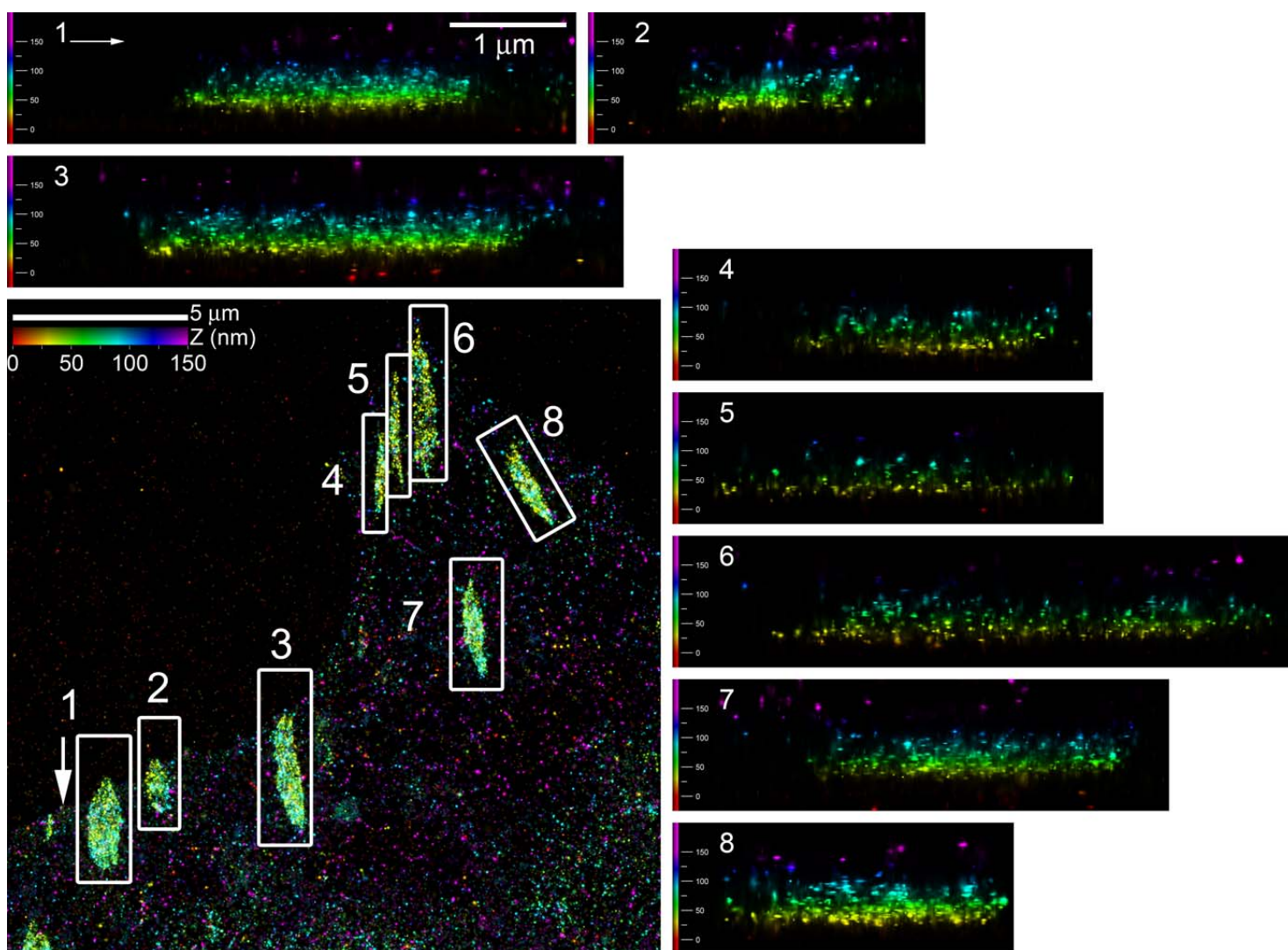
Supplementary Figure 13. Paxillin

Topview iPALM image (**left**) of paxillin-tdEos (Paxillin-C) in U2OS cell. Sideview projections (right) are shown for boxed areas (**1-8**), same color scale as topview. Z coordinates relative to substrate surface (0-150 nm) indicated by color bar (left) and vertical scale (sideviews). Arrows indicate sideview orientation. All sideviews are on the same scale (scale bar, 1 μm). Area 5 corresponds to Fig. 2d. Paxillin-tdEos localized to a narrow plane at $z \sim 40\text{-}45$ nm from the substrate surface.



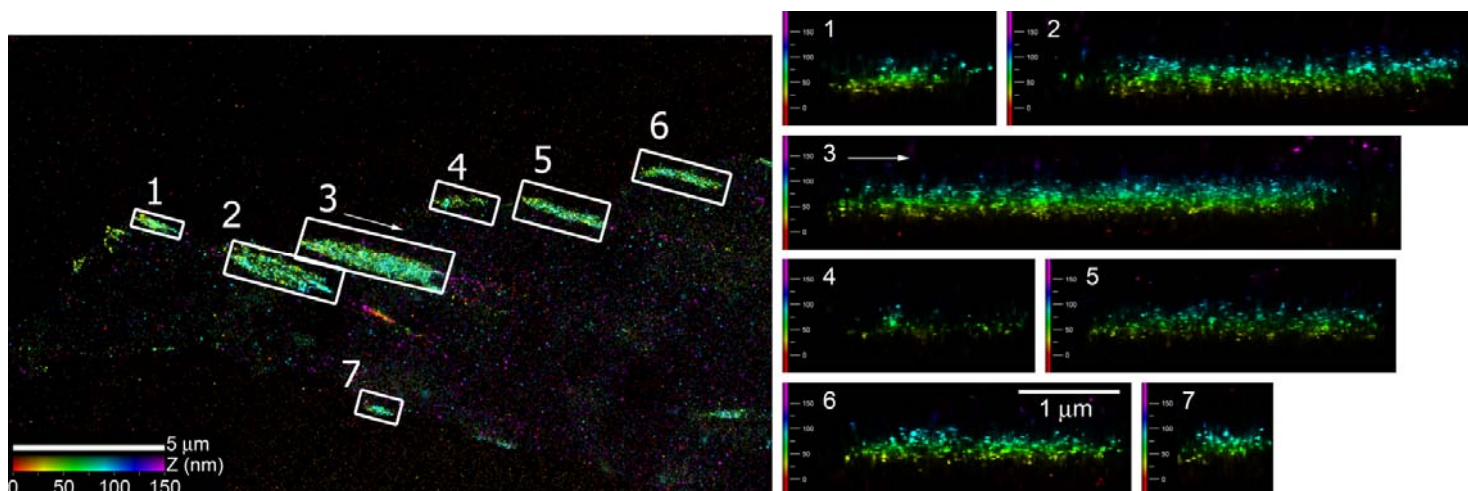
Supplementary Figure 14. Vinculin

Topview iPALM image (**left**) of vinculin-tdEos in U2OS cell. Sideview projections (right) are shown for boxed areas (**1-8**), same color scale as topview. Z coordinates relative to substrate surface (0-150 nm) indicated by color bar (left) and vertical scale (sideviews). Arrows indicate sideview orientation. All sideviews are on the same scale (scale bar, 1 μm). Area 1 corresponds to Fig. 2f. Vinculin-tdEos localizations are observed with maximum density at $z \sim 50\text{-}60\text{ nm}$ from the substrate surface.



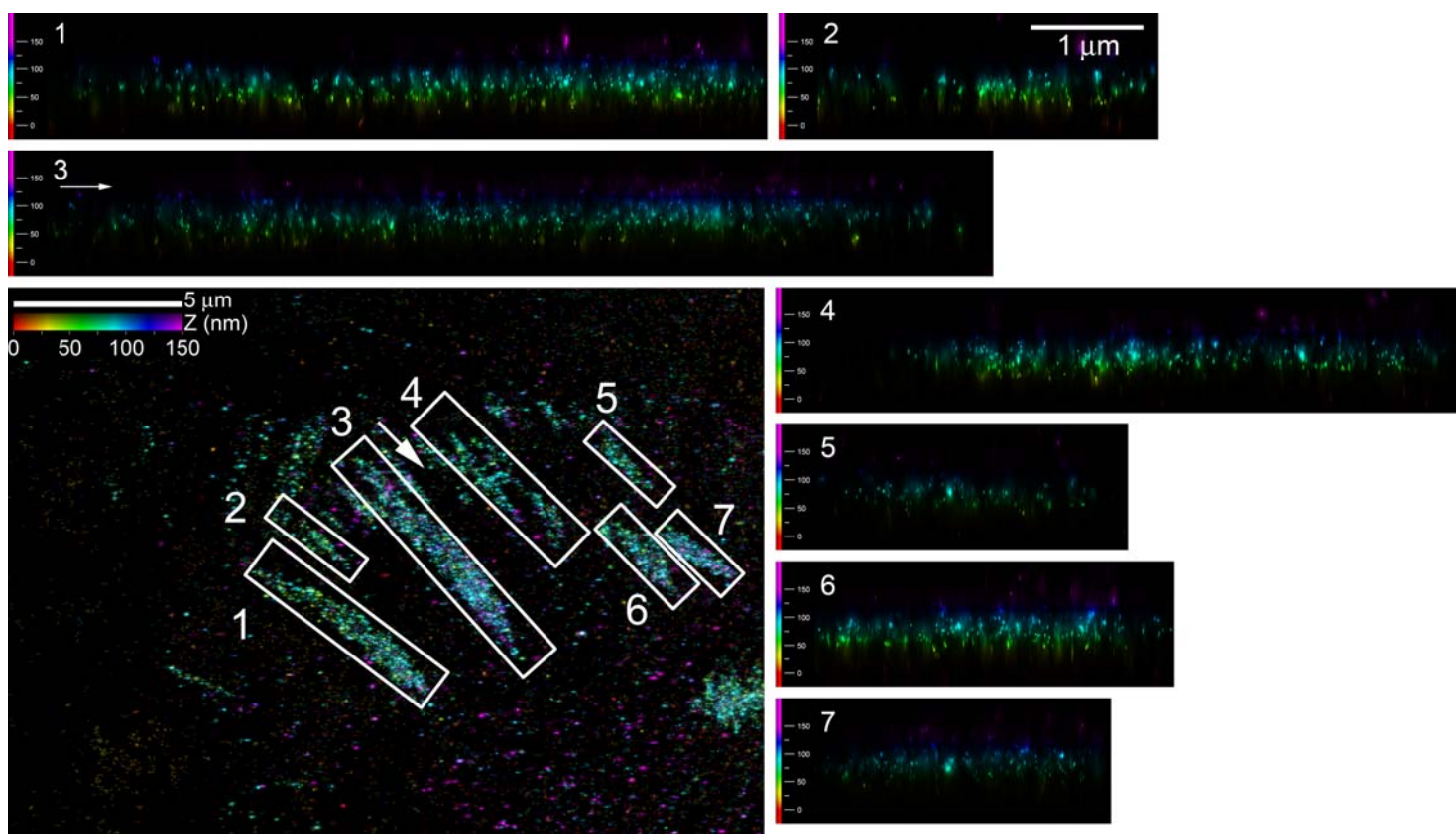
Supplementary Figure 15. Zyxin

Topview iPALM image (**left**) of zyxin-mEos2 in U2OS cell. Sideview projections (right) are shown for boxed areas (**1-7**), same color scale as topview. Z coordinates relative to substrate surface (0-150 nm) indicated by color bar (left) and vertical scale (sideviews). Arrows indicate sideview orientation. All sideviews are on the same scale (scale bar, 1 μm). Area 2 corresponds to Fig. 2h. Zyxin-mEos2 localizations are observed with maximum density at $z \sim 70\text{-}80\text{ nm}$ from the substrate surface.



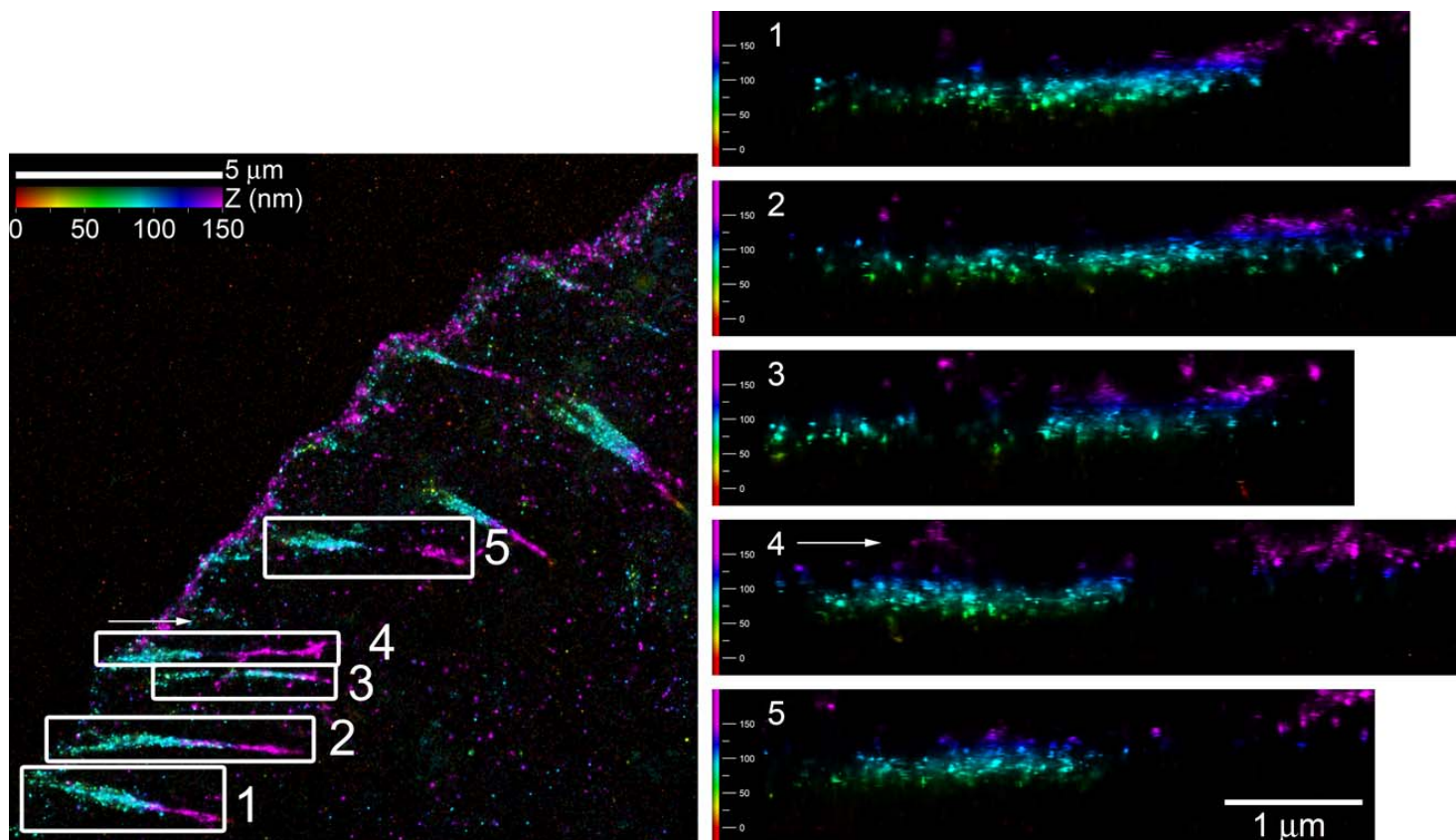
Supplementary Figure 16. VASP

Topview iPALM image (**bottom left**) of VASP-mEos2 in U2OS cell. Sideview projections (right) are shown for boxed areas (**1-7**), same color scale as topview. Z coordinates relative to substrate surface (0-150 nm) indicated by color bar (left) and vertical scale (sideviews). Arrows indicate sideview orientation. All sideviews are on the same scale (scale bar, 1 μm). Area 3 corresponds to Fig. 2j. VASP-mEos2 localizations are observed with maximum density at $z \sim 70\text{-}90$ nm from the substrate surface.



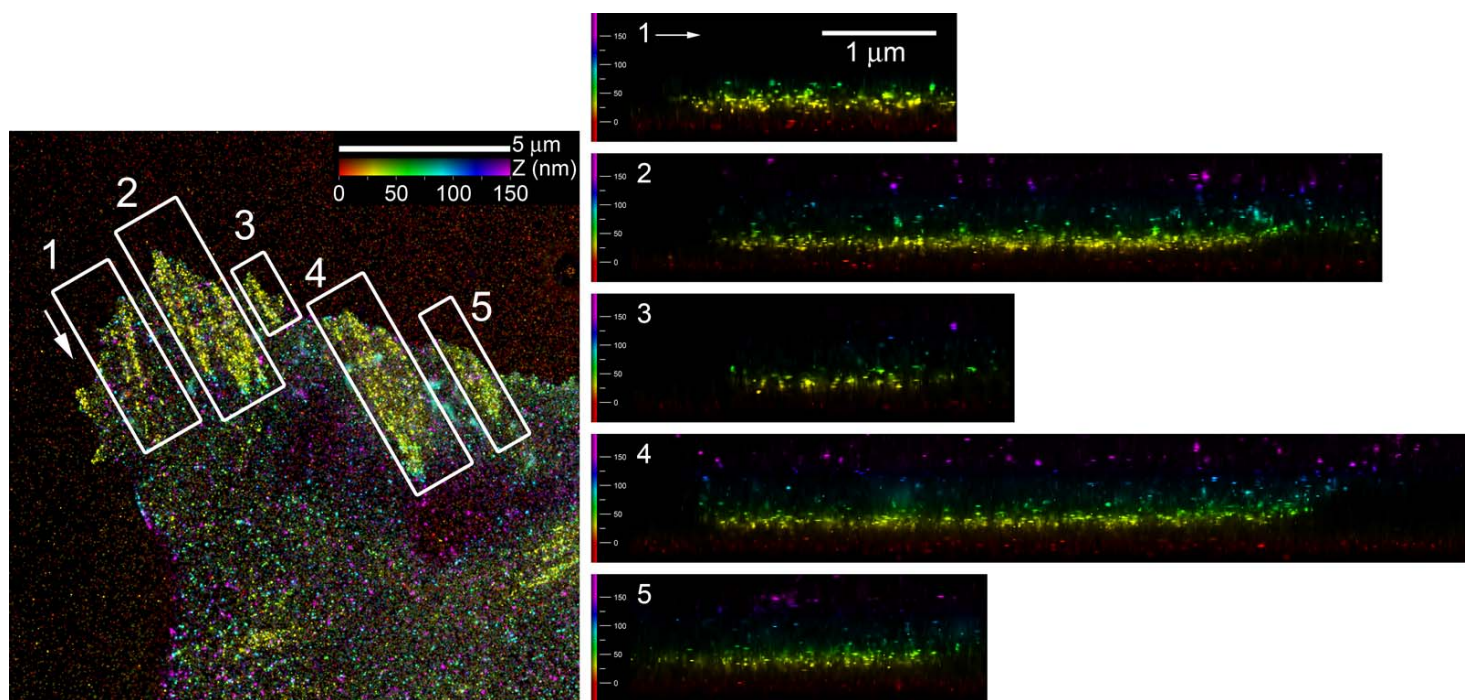
Supplementary Figure 17. α -actinin

Topview iPALM image (**left**) of α -actinin-mEos2 (α -actinin-C) in U2OS cell. Sideview projections (right) are shown for boxed areas (**1-5**), same color scale as topview. Z coordinates relative to substrate surface (0-150 nm) indicated by color bar (left) and vertical scale (sideview). Arrows indicate sideview orientation. All sideviews are on the same scale (scale bar, 1 μ m). Area 2 corresponds to Fig. 2I. α -actinin-mEos2 localizations in the adhesions appear similar to the distribution of actin in stress fibers, virtually excluded from lower z. Lamellipodial localization of α -actinin-mEos2 is also observed at the cell edge at z~100 nm or greater.



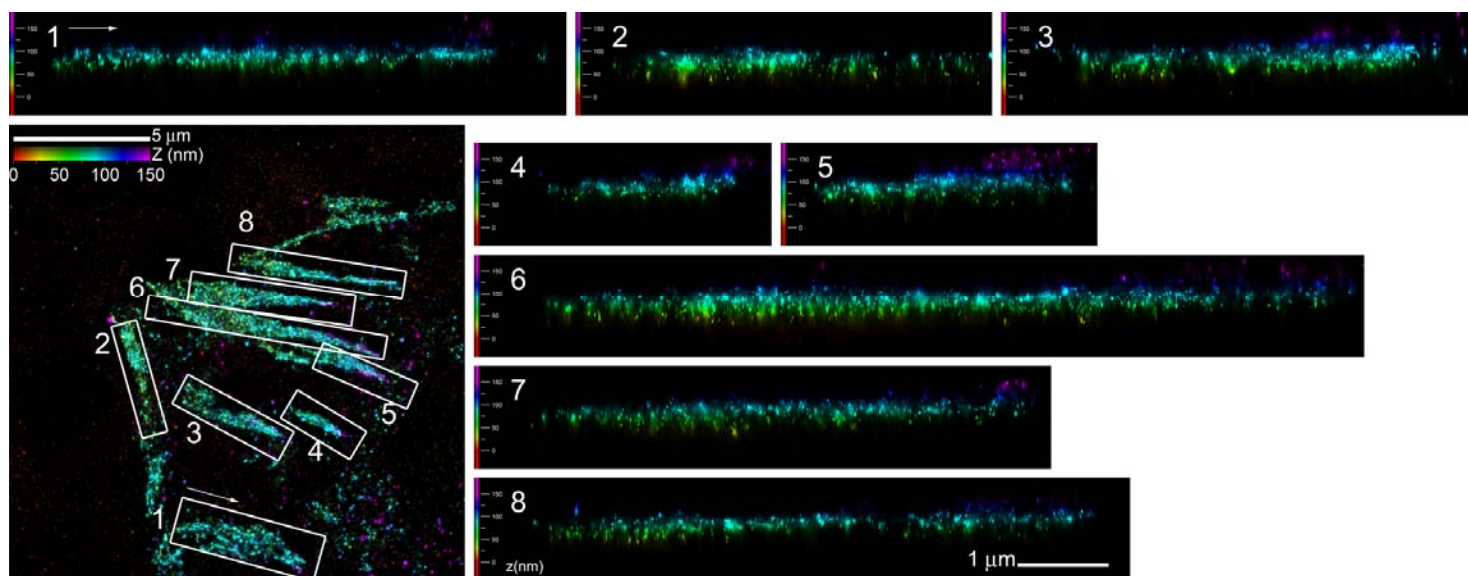
Supplementary Figure 18. Talin-N

Topview iPALM image (**left**) of Talin-N (tdEos-18-Talin) in U2OS cell. Sideview projections (right) are shown for boxed areas (**1-5**) with the same color code as topview. Z coordinates relative to substrate surface (0-150 nm) indicated by color bar (left) and vertical scale (sideview). Arrows indicate sideview orientation. All sideviews are on the same scale (scale bar, 1 μm). Area 2 corresponds to Fig. 3c. Talin-N localizations are observed in a narrow band at $z \sim 40$ nm from the substrate surface.



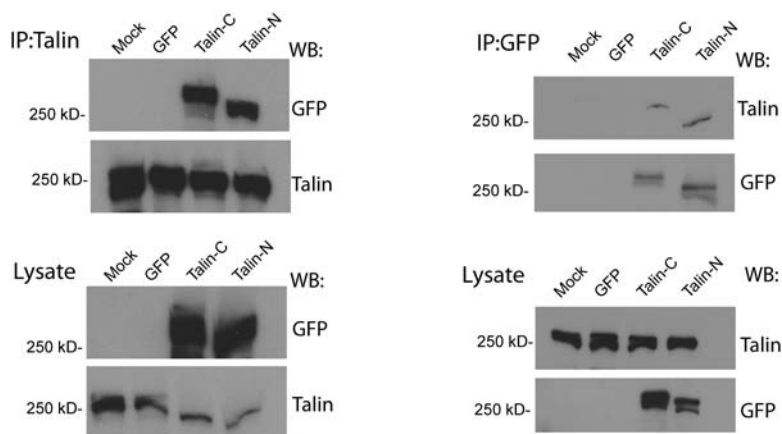
Supplementary Figure 19. Talin-C

Topview iPALM image (**left**) of Talin-C (Talin-22-tdEos) in U2OS cell. Sideview projections (right) are shown for boxed areas (**1-8**) with the same color code as topview. Z coordinates relative to substrate surface (0-150 nm) indicated by color bar (left) and vertical scale (sideview). Arrows indicate sideview orientation. All sideviews are on the same scale (scale bar, 1 μm). Area 5 and 7 correspond to Figure 3e and 3f, respectively. Talin-C localizations are observed confined to a layer at $z \sim 70$ nm or greater, and are virtually excluded from lower z .



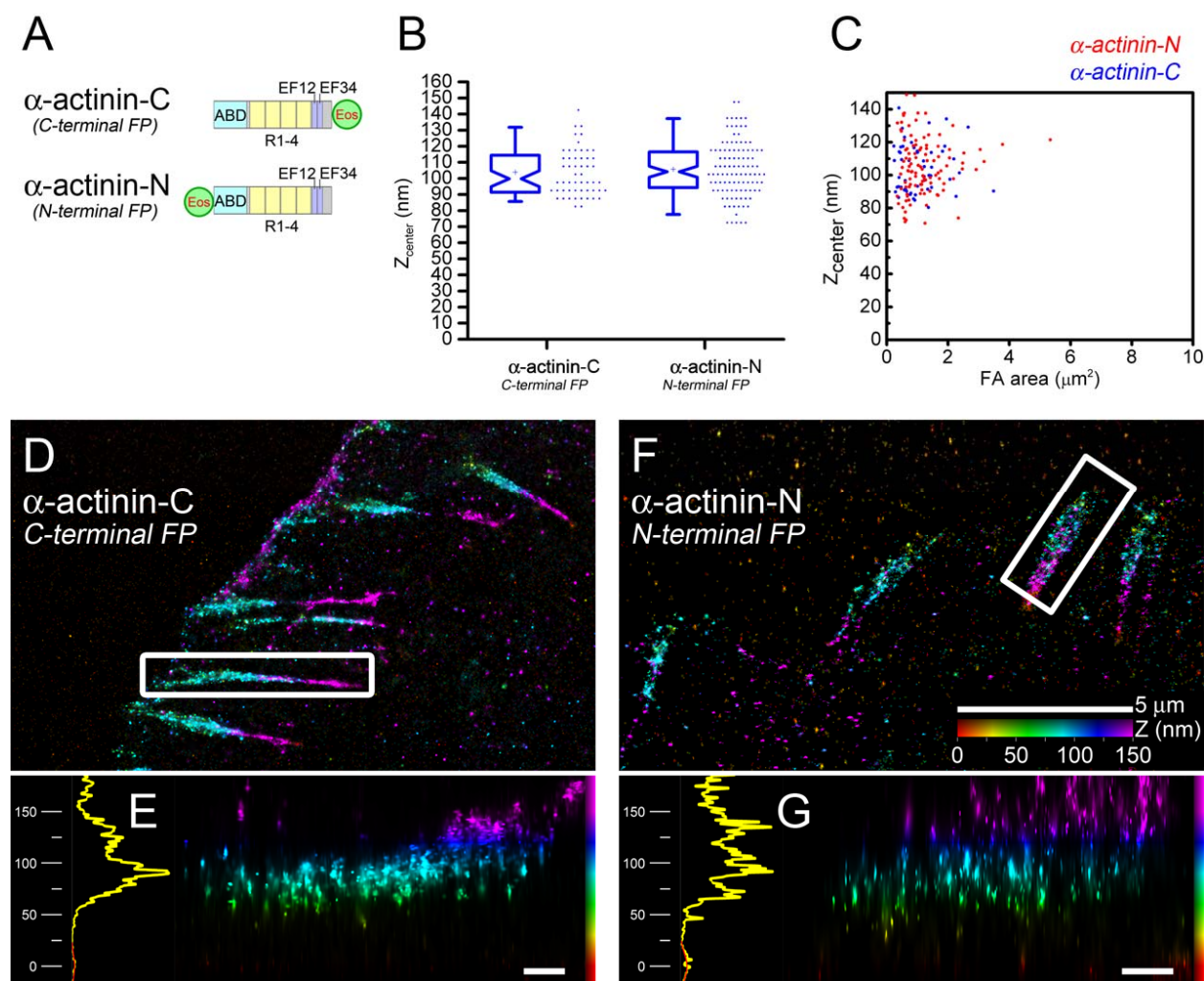
Supplementary Figure 20. Expressed talin constructs co-immunoprecipitates with endogenous Talin

Immunoprecipitations were performed from lysates of non-transfected U2OS cells (mock), or cells transfected with GFP control vector, Talin-C, and Talin-N. **(Left)** IP of endogenous Talin with anti-human Talin antibody that does not recognize mouse Talin in the –N and –C fusion constructs. Top panels show immunoblot results with anti-GFP, and the stripped and blotted results with anti-human Talin. GFP-tagged Talin-N and Talin-C is pulled down by endogenous talin. Total protein inputs from lysates are shown in bottom panels. **(Right)**, IP of Talin-N and Talin-C constructs with anti-GFP antibodies. Top panels show immunoblot results with anti-human talin, and the stripped and blotted results with anti-GFP. Endogenous talin is pulled down by both Talin-C and Talin-N constructs. Total protein inputs from lysates are shown in bottom panels.



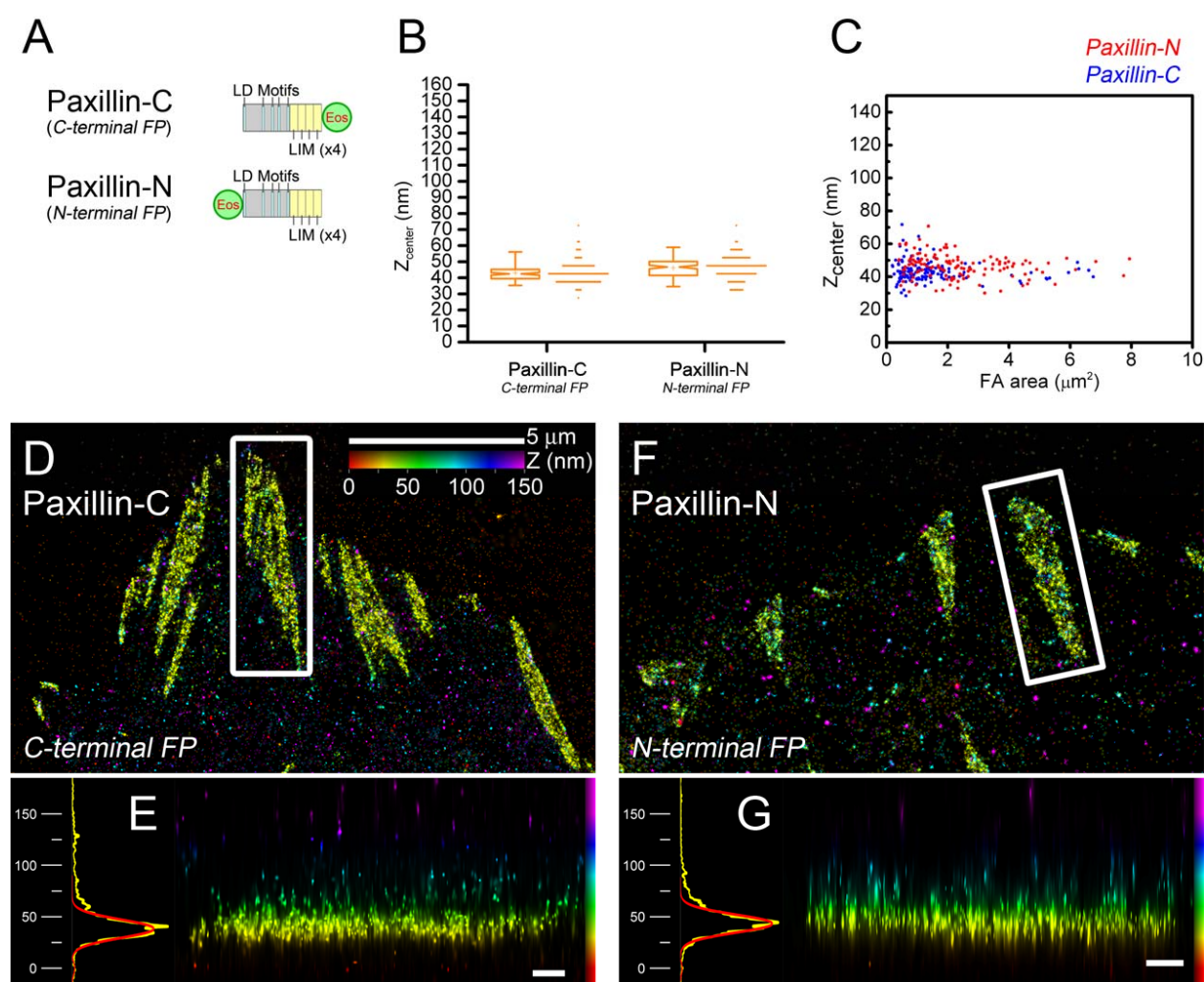
Supplementary Figure 21. α -actinin C and N terminal localization in focal adhesions

(A) schematic diagram of α -actinin fusion constructs showing the positions of the PA-FP probe (Eos: mEos2) at either termini of full-length α -actinin: C-terminus (α -actinin-C, shown in Fig. 2, and Supplementary fig. 17), or N-terminus (α -actinin-N). Domain names indicated (ABD: actin binding domain, R1-4: spectrin repeat, EF12 and EF24: EF hand motifs). **(B)** peak position, z_{center} (peak of Gaussian distribution or 1st moment) of α -actinin-C or -N in FAs. Notched boxes: 1st & 3rd quartiles, median, and confidence interval; whiskers: 5th and 95th percentiles; +: means. Individual data points also shown to the right with 5-nm binning, center justified. Additional parameters shown in Supplementary Table 1. **(C)** Plot of z_{center} protein positions (nm) as a function of FA area (μm^2) for α -actinin-C (blue) or α -actinin-N (red). Each point represents an FA region. **(D, F)** Topview iPALM images of U2OS cells expressing PA-FP fusion protein probes (D, E from Fig. 2). **(E, G)** Sideview projections (right), histograms (1-nm bins) of molecular positions (left, yellow plots) in FA areas (white boxes in D, F), and Gaussian fits (red) for substratum level. Color in D-G indicates the vertical (z) coordinate relative to the substrate ($z = 0$ nm, red). Scale bars, 5 μm in (D, F), 500 nm in (E, G).



Supplementary Figure 22. Paxillin C and N terminal localization in focal adhesions

(A) schematic diagram of paxillin fusion constructs showing the positions of the PA-FP probe (Eos: tdEos) at either termini of full-length paxillin: C-terminus (Paxillin-C, shown in Fig. 2, and Supplementary fig. 13), or N-terminus (Paxillin-N). **(B)** peak position, z_{center} (peak of Gaussian distribution or 1st moment) of Paxillin-C or -N in FAs. Notched boxes: 1st & 3rd quartiles, median, and confidence interval; whiskers: 5th and 95th percentiles; +: means. Individual data points also shown to the right with 5-nm binning, center justified. Additional parameters shown in Supplementary Table 1. **(C)** Plot of z_{center} protein positions (nm) as a function of FA area (μm^2) for Paxillin-C (blue) or Paxillin-N (red). Each point represents an FA region. **(D, F)** Topview iPALM images of U2OS cells expressing PA-FP fusion protein probes (D, E from Fig. 2). **(E, G)** Sideview projections (right), histograms (1-nm bins) of molecular positions (left, yellow plots) in FA areas (white boxes in D, F), and Gaussian fits (red). Color in D-G indicates the vertical (z) coordinate relative to the substrate ($z = 0$ nm, red). Scale bars, 5 μm in (D, F), 500 nm in (E, G).



Supplementary Tables 1-4

Supplementary Table 1. Statistics of FA protein vertical distributions

Vertical distributions of proteins in individual FAs were characterized by z_{center} and width parameter (σ_{vert}) determined from Gaussian fits to histograms of FA and coverglass surface localizations (Supplementary fig. 3). Box plots shown in fig. 4a-b. Individual FA data points shown in fig. 4c and Supplementary fig. 9 as a function of area or FA aspect ratio. The localizations of actin and α -actinin exhibit tapered profiles and non-Gaussian distributions, so the 1st and 2nd moment were calculated instead of Gaussian fittings. Note that for a Gaussian distribution, full-width-half-maximum (FWHM) = $2.35 \cdot \sigma_{vert}$. Number of total FA localizations ($N_{localizations}$), number of FAs (N_{FA}), and number of cells (N_{cell}) used in the analysis are shown.

FA proteins	Average $z_{center} \pm$ st. dev. (nm)	Average $\sigma_{vert} \pm$ st. dev. (nm)	$N_{localizations}$	N_{FA}	N_{cell}
Integrin α_v	36.8 ± 4.5	7.2 ± 1.8	1.05×10^6	75	9
FAK	36.0 ± 4.7	10.0 ± 2.5	1.23×10^6	112	7
Paxillin-C	43.1 ± 6.1	8.6 ± 2.8	1.15×10^6	138	9
Paxillin-N	46.2 ± 7.1	11.6 ± 3.1	1.24×10^6	131	9
Talin-N	42.8 ± 3.8	9.8 ± 2.4	1.02×10^6	110	10
Talin-C	76.7 ± 10.6	15.7 ± 3.8	1.31×10^6	56	8
Vinculin	53.7 ± 5.5	13.1 ± 3.9	2.22×10^6	232	17
Zyxin	73.2 ± 8.8	17.5 ± 3.5	1.77×10^6	142	8
VASP	80.5 ± 11.6	23.4 ± 4.5	1.04×10^6	123	8
α -actinin-C	103.9 ± 14.6	22.8 ± 5.1	9.18×10^5	54	6
α -actinin-N	105.7 ± 17.3	25.6 ± 8.0	9.16×10^5	106	7
Actin	96.9 ± 15.2	31.0 ± 8.7	1.26×10^6	57	11

Supplementary Table 2. Vertical localization parameters for FA regions in Figures 1-3

Fit parameters for vertical protein distribution for selected FA areas shown in Figures 1-3. The center vertical position (z_{center}) and width parameter (σ_{vert}) are shown \pm s.e.m. N denotes the number of localizations in each peak.

Proteins	FA			Substrate		
	$Z_{center} \pm \text{s.e.m. (nm)}$	$\sigma_{vert}(\text{nm})$	N	$Z_{center} \pm \text{s.e.m. (nm)}$	$\sigma_{vert}(\text{nm})$	N
Integrin α_v	35.24 \pm 0.03	5.31	22193	0 \pm 0.43	14.68	1151
FAK	32.24 \pm 0.05	9.16	26542	0 \pm 0.36	5.46	223
Paxillin	38.51 \pm 0.05	8.01	25797	0 \pm 0.26	5.87	521
Talin-N	39.11 \pm 0.06	8.79	23041	0 \pm 0.13	7.03	2785
Talin-C (3e)	82.81 \pm 0.09	16.56	33192	0 \pm 0.51	5.98	139
Talin-C (3f)	76.84 \pm 0.15	20.59	18886	0 \pm 0.86	9.00	109
Vinculin	54.30 \pm 0.10	14.19	19036	0 \pm 0.31	6.49	437
Zyxin	72.00 \pm 0.12	19.12	27365	0 \pm 0.34	9.78	822
VASP	93.91 \pm 0.15	26.81	33141	0 \pm 0.59	6.64	125
α -actinin	97.29 \pm 0.09	20.16	45287	0 \pm 0.39	10.55	749
Actin	117.10 \pm 0.25	63.57	64271	0 \pm 0.26	6.95	727

Supplementary Table 3. PA-FP fusion protein expression constructs

The constructs are denoted by [FP-linker-protein] or [Protein-linker-FP] for probes with FP at the N-terminus or C-terminus, respectively; linker lengths in amino acids indicated. Schematic diagram of the probes are shown in Supplementary fig. 4 with micrographs of cellular localization shown in Supplementary fig. 5. Functional classification and reported interactions, according to the database in Ref.4, are shown for proteins used in this study and other important proteins.

Functional Category	Components	PA-FP fusion constructs	Reported Interactions in FAs
Plasma membrane marker	CAAX	tdEos-5-[c-Ha-Ras CAAX]	Target to cytoplasmic leaflet of plasma membrane
Cell-ECM Adhesion	Integrin α_v	Integrin α_v -25-tdEos	Extracellular domain ($\alpha_v\beta_3$): fibronectin, fibrillin, fibrinogen, tenascin Cytoplasmic domain: 13 (α) / 31 (β) proteins including talin, FAK, paxillin, α -actinin
Integrin Signaling	FAK	tdEos-5-FAK	42 proteins including integrin, talin, paxillin, Grb2, Csk, and Fyn
	Paxillin	Paxillin-22-tdEos (Paxillin-C) tdEos-10-Paxillin (Paxillin-N)	36 proteins including FAK, vinculin, integrin, Src, and ILK
Cytoskeletal Adaptor	Talin	tdEos-18-Talin1 (Talin-N) Talin1-22-tdEos (Talin-C) mEos2-7-TalinABS (THATCH) tdEos-18-TalinHead (Head)	12 proteins including vinculin, actin, integrin, FAK, paxillin THATCH domain: actin Head domain: integrin, actin, FAK, paxillin, Layilin
	Vinculin	tdEos-14-Vinculin	15 proteins including talin, actin, VASP, paxillin, α -actinin
	Zyxin	Zyxin-6-mEos2	9 proteins including VASP and α -actinin.
Actin associated	VASP	mEos2-5-VASP	13 proteins including zyxin, actin, α -actinin, and vinculin
	α -actinin	α -actinin-19-mEos2 (α -actinin-C) mEos2-14- α -actinin (α -actinin-N)	18 proteins including actin, vinculin, zyxin, VASP, and integrin
Cytoskeletal components	Actin	mEos2-7-actin	23 proteins including talin, vinculin, VASP, and α -actinin

Supplementary Table 4. Imaging parameters

PA-FP fusion constructs and number of image triplets used for each iPALM data set.

Figures	Cell Type	PA-FP fusion constructs	# frame triplets
Figure 1a-c, Supplementary Fig. 2	U2OS	tdEos-5-[c-Ha-Ras CAAX]	60,000
Figure 1d-e, Supplementary Fig. 6	U2OS	Integrin α_v -25-tdEos	25,000
Figure 1f-g, Supplementary Fig. 7	U2OS	mEos2-7-actin	75,000
Figure 2a-b, Supplementary Fig. 12	U2OS	tdEos-5-FAK	25,000
Figure 2c-d, Supplementary Fig. 13, 22D-E	U2OS	Paxillin-22-tdEos	25,000
Figure 2e-f, Supplementary Fig. 3, 14	U2OS	tdEos-14-Vinculin	25,000
Figure 2g-h, Supplementary Fig. 15	U2OS	Zyxin-6-mEos2	25,000
Figure 2i-j, Supplementary Fig. 16	U2OS	mEos2-5-VASP	50,000
Figure 2k-l, Supplementary Fig. 17, 21D-E	U2OS	α -actinin-19-mEos2	75,000
Figure 3b-c, Supplementary Fig. 18	U2OS	tdEos-18-Talin1	25,000
Figure 3d-f, Supplementary Fig. 19	U2OS	Talin1-22-tdEos	40,000
Supplementary Fig. 1C	U2OS	tdEos-14-Vinculin	25,000
Supplementary Fig. 8	U2OS	mEos2-7-actin	25,000
Supplementary Fig. 10A-B	MEF	Integrin α_v -25-tdEos	25,000
Supplementary Fig. 10C-D	MEF	mEos2-7-actin	35,000
Supplementary Fig. 10E-F	MEF	Paxillin-22-tdEos	40,000
Supplementary Fig. 10G-H	MEF	tdEos-14-Vinculin	25,000
Supplementary Fig. 10I-J	MEF	tdEos-18-Talin1	25,000
Supplementary Fig. 10K-L	MEF	Talin1-22-tdEos	25,000
Supplementary Fig. 11A-B	U2OS	tdEos-18-TalinHead	25,000
Supplementary Fig. 11C-D	U2OS	mEos2-7-THATCH	50,000
Supplementary Fig. 21F-G	U2OS	mEos2-14- α -actinin	25,000
Supplementary Fig. 22F-G	U2OS	tdEos-10-Paxillin	25,000

Supplementary Note 1

Optical Configuration of interferometric Photo-Activated Localization Microscope (iPALM) setup

A schematic diagram of the iPALM optical setup is shown in Supplementary fig. 1. The samples for imaging were assembled as described in Methods and placed between two opposing infinity-corrected microscope objective lenses (Nikon CFI Apochromat TIRF 60x, NA=1.49, Nikon Instruments Inc., Melville, NY); index matching oil was used (Cargille type DF, Cargille Laboratories, Cedar Grove, NJ). We used light from a 50 mW 405 nm diode laser (Coherent Inc., Santa Clara, CA), attenuated by neutral density filters to low intensity, for single fluorophore level activation of the photoconvertible fluorescent proteins, and 150 mW 561 nm diode pumped solid-state laser (CrystaLaser, Reno, NV) for excitation of activated fluorescent proteins. Narrow bandwidth laser line filters (MaxLine[®] LL01-561-12.5 and MaxDiode[®] LD01-405/10-12.5, Semrock Inc., Rochester, NY) were used to reject both emission noise from the laser and autofluorescence generated in the optical path prior to the objectives. The activation and excitation beams entered the back pupil planes of the objectives through the slots in the custom turning mirrors (Reynard Corp., San Clemente, CA). The radial position of these beams was controlled to produce a near-total internal reflection (TIR) condition, whereby the ratio of optical powers of transmitted through the chamber to that reflected by the chamber was less than 5%. The fluorescence signal was collected by the infinity-corrected objective lenses and the image-forming beams were interfered in the 3-way beamsplitter custom manufactured by Rocky Mountain Instruments (Lafayette, CO). The output beams from the 3-way beam splitter were then focused on 3 separate EMCCD cameras (Andor iXon DU-897, Andor Technology, Belfast, Northern Ireland) via f=400 mm achromatic lenses (01LAO799, CVI Melles Griot, Albuquerque, NM). In order to reject the excitation light, we used the long-pass and band-pass optical filters (RazorEdge[®] LP02-568RU-25 and BrightLine[®] FF01-588/21-25, Semrock Inc., Rochester, NY).

Supplementary Note 2

Correlation of iPALM with Immunofluorescence Microscopy

To characterize the substrate on which the cells were grown and to verify that expressed PA-FP fusions were co-localizing with endogenous FA proteins, correlative iPALM-immunofluorescence were carried out. iPALM samples were prepared and imaged as described earlier. The rough coordinate of the sites imaged by iPALM were recorded, providing the position of the imaged cells relative to one another. After iPALM imaging, excess immersion oil was removed and the epoxy bonding of the sample coverglasses was pried open under PHEM buffer, using a thin stainless steel shim (12-25 μm , McMaster, CA). The opened sample was then briefly refixed for 5-10 minutes in 2 % paraformaldehyde at room temperature, permeabilized for 15 minutes in 0.1 % Triton X-100, quenched for 15 minutes in 50 mM glycine, and blocked for 1 hour in 1% BSA. The sample was incubated for 1 hour with rabbit anti-fibronectin antibody (Sigma Aldrich F-3648, 1:200 dilution in 1% BSA PHEM buffer) and mouse anti-paxillin antibody (P13520, BD Bioscience), followed by 1-hour incubation with Cy2-Donkey anti-rabbit secondary antibody (Jackson ImmunoResearch 111-225-003), Cy3 Donkey anti-mouse secondary antibody (715-165-150 Jackson ImmunoResearch), and Alexa647 Phalloidin (A22287, Invitrogen), and mounted using Dako mounting media (S3023, Dako) and allowed to harden overnight.

Hard-mount samples were positioned on ASI-2000 XY stage, and a mosaic of images of the entire sample was scanned in the Cy3 paxillin channel. The microscope used was a Nikon TE2000 with a Nikon 40X NA 1.3 oil immersion objective and a Coolsnap HQ² camera (Photometrics, Tucson, AZ) with 2x2 binning. Each sub-image of the mosaic was taken at 100 μm step of X,Y –stage movement. The individual images were then cropped and stitched together in ImageJ, yielding a mosaic covering 20-40 mm^2 area, with high enough resolution to identify cellular details. A visual scan identified cells that has been imaged by iPALM based on the focal adhesions patterns and their relative position among the imaged cells. The coordinates of the cells were noted and higher magnification immunofluorescence micrographs were obtained using a Nikon 60X Apo TIRF NA 1.49 oil-immersion objectives, with a CoolSnap HQ² camera without binning. To match the different scale of Immunofluorescence to iPALM images, the images were rescaled in Photoshop CS3. Note that the FA “footprint” seen in the fibronectin immunofluorescence image (Supplementary Fig. 3E) is due to steric exclusion and epitope masking by integrin and other ECM receptors, similar to an earlier observation³⁶.

Supplementary Note 3

Mammalian Expression Vectors.

All photoactivatable fluorescent protein (PA-FP) expression vectors were constructed using C1 and N1 (Clontech™-style) cloning vectors. In most cases, we started with EGFP (enhanced green fluorescent protein) fusion constructs that have been previously characterized biochemically and/or cell biologically in the literature. A summary of functional categories, binding interactions, and the specific PA-FP used for each construct (either tandem dimer EosFP (tdEos)¹⁸ or monomeric mEos2¹⁹), and linker lengths are listed in Supplementary Table 3. We used tdEos where the expressed proteins localize properly since it offers optimal photophysical properties. However, in some cases, such as VASP and α -actinin, tdEos fusion caused partial aggregation of expressed proteins, and mEos2 constructs which localize properly, were used instead.

All DNA for transfection was prepared using the Plasmid Maxi kit (QIAGEN, Valencia, CA). To ensure proper localization, mEos2 and tdEos fusion proteins were characterized by transfection in HeLa cells (CCL2 line; ATCC, Manassas, VA) using Effectene (QIAGEN) and ~1 μ g vector. Transfected cells were grown on coverglasses in DMEM/F12, fixed after 48 hours, and mounted with Gelvatol. Epifluorescence images (Supplementary Fig. 5) were taken with a Nikon 80i microscope using widefield illumination and a FITC filter set, showing proper localizations.

The PA-FP cDNA (mEos2 or tdEos) was amplified with a 5' primer encoding an AgeI site and a 3' primer encoding either a BspEI (C1) or NotI (N1) site for C-terminal and N-terminal fusions (with regards to the FP), respectively. The purified and digested PCR products were ligated into similarly digested EGFP-C1 and EGFP-N1 cloning vector backbones. To generate fusion vectors, the appropriate cloning vector and an EGFP fusion vector were digested, either sequentially or doubly, with the appropriate enzymes and ligated together after gel purification. Thus, to prepare mEos2 and tdEos N-terminal fusions (FP and number of linker amino acids in parenthesis), the following digests were performed: human non-muscle α -actinin (mEos2; 19), EcoRI and NotI (α -actinin cDNA source, Tom Keller, Florida State University); chicken paxillin (tdEos; 22), EcoRI and NotI (paxillin cDNA source, Alan Horwitz, University of Virginia); human α_v integrin (tdEos; 25), AgeI and NotI (α_v integrin cDNA source, Alan Horwitz, University of Virginia); human zyxin (mEos2; 6), BamHI and NotI (zyxin cDNA source, OriGene Technologies, Rockville, MD);

To prepare mEos2 and tdEos C-terminal fusions (FP and number of linker amino acids in parenthesis), the following digests were performed: human β -actin (mEos2; 7), NheI and BglII (β -actin DNA source, Clontech, Mountain View, CA); human vinculin (tdEos; 14), NheI and EcoRI (vinculin cDNA source, Open Biosystems, Huntsville, AL); chicken focal adhesion kinase (tdEos; 5), AgeI and BglII (focal adhesion kinase cDNA source, Alan Horwitz, University of Virginia); mouse vasodilator-stimulated phosphoprotein (VASP) (mEos2, 5), NheI and BglII (VASP cDNA source, Frank Gertler, MIT), CAAX-containing 20-amino acid farnesylation signal from c-Ha-Ras (tdEos; 5), AgeI and BspEI (farnesyl signal peptide DNA source, Clontech, Mountain View, CA).

EGFP fused to the N-terminus of mouse talin1 and housed in a standard C1-Clontech style vector (EGFP-18-talin) was a generous gift of Dr. Anna Huttenlocher (University of Wisconsin, Madison). Site-directed mutagenesis (QuickChange Lightning; Stratagene, La Jolla, CA) was used to remove a BspEI site from mouse talin1 (nucleotides 269-274) for cloning. The products of a digestion of EGFP-18-talin and the tdEos-C1 with AgeI and BspEI were ligated to yield tdEos having mouse talin1 fused to the C-terminus separated by an 18 amino acid linker, denoted Talin-N.

An EGFP variant (mEmerald) was used to produce a mouse talin1 fusion with the FP linked to the N-terminus. Thus, the following primers were used to amplify the N-terminal 4,021 nucleotides of mouse talin 1 and create EcoRI and XmaI restriction sites:

EcoRI forward: **GAC GGT AGA ATT CTA GCC ACC ATG GTT GCG CTT TCG CTG AAG ATT AGC ATT GG**

XmaI reverse: **TCC GTC ACT GCC CGG GCA GCC GCA GCC AGC TGA CTC TTG AGG TTG GGA GAA G**

The PCR product was ligated into a similarly cut mEmerald-N1 cloning vector. Next, the following primers were used to amplify the C-terminal 3,608 nucleotides of mouse talin1 and create XmaI and AgeI restriction sites:

XmaI forward: **GAT TCA TCG CCC GGG CAG TGA CGG ACA GCA TCA ACC AGC TC**

AgeI reverse: **GGT GGC GAC CGG TGA TCG GGA CGC GGA GCC TGC GCC GGA CCC TTG CCC GGA CCC GGA CCC AGC GCC GTG CTC GTC TCG AAG CTC TGA AGG C**

This PCR product was ligated into the mEmerald-N1 vector containing the EcoRI and XmaI insert to yield a fusion of mEmerald and mouse talin1 (N-terminal with respect to mEmerald) separated by a 22 amino acid linker. This vector along with tdEos-N1 was digested using AgeI and NotI. The products were ligated to produce talin-22-tdEos, denoted Talin-C.

The Talin-head domain (amino acids 1-433) of mouse talin1 fused to the C-terminus of EGFP in a Clontech vector was a gift from Dr. Anna Huttenlocher. EGFP was replaced by tdEos by digestion of the appropriate vector and tdEos-C1 with AgeI and BspEI, followed by ligation of tdEos into the vector backbone. The 197-amino acid C-terminal actin binding domain (THATCH) of talin was created by amplifying EGFP-18-talin to introduce BglII and BamHI restriction enzyme sites using the following primers:

BglII forward: **TCC GGA CTC AGA TCT CGA GCT CAA GCT TCG ATC CTA GAA GCT GCC AAG TCC ATC GCT G**

BamHI reverse: **TCC GGT GGA TCC TTA GTG CTC GTC TCG AAG CTC TGA AGG C**

The PCR product and EGFP-C1 were digested with BglII and BamHI, and the products were ligated to yield EGFP-7-TalinTHATCH. mEos2 was substituted for EGFP using AgeI and BspEI with mEos2-C1 and EGFP-7-TalinTHATCH.

To transfer fluorescent protein fusions to the N-terminus of α -actinin, the vector mEmerald- α -actinin-19 was amplified using the following primers to introduce XhoI and EcoRI restriction sites:

XhoI forward: **CTC AGA TCT CGA GGA AGC GGC GGA TCT GGG TCC GGA GAC CAT TAT GAT TCT CAG CAA ACC AAC GAT TAC ATG CAG CCA G**

EcoRI reverse: **CGG TAC CTG AAT TCT TAG AGG TCA CTC TCG CCG TAC AGC GCC**

The PCR product and mEmerald-C1 were digested with XhoI and EcoRI, and the products were ligated to yield mEmerald-14- α -actinin. mEos2 was substituted for mEmerald using NheI and XhoI with mEos2-C1 and mEmerald-14- α -actinin.

Since chicken paxillin contains alternate splice site, for the N-terminal FP tagged version of paxillin, we use a paxillin construct with the T132S and M133L mutations which eliminate a Kozak sequence responsible for the splicing, as described previously³⁷. To transfer fluorescent protein fusions to the N-terminus of the unspliced version of paxillin, the vector EGFP-10-Paxillin was amplified using the following primers to introduce BglII and BamHI restriction sites:

BglII forward: **TCC GGA CTC AGA TCT GGC AGC AGT GGA GGT GAC GAC CTC GAT GCC TTA CTG GCA GAC C**

BamHI reverse: **TCC GGT GGA TCC TTA ACA GAA GAG TTT GAG AAA GCA GTT CTG ACA GTA GGG CTT GTC G**

The PCR product and mEmerald-C1 were digested with BglII and BamHI, and the products were ligated to yield mEmerald-10-Paxillin. tdEos was substituted for mEmerald using NheI and BglII with tdEos-C1 and mEmerald-10-Paxillin.

For iPALM imaging of PA-FP constructs, transfections were carried out by electroporation using Amaxa nucleofector (Lonza, Cologne, Germany) and plated on imaging coverglasses as described above. The tdEos-fused integrin α_v was co-transfected in 1:1 ratio with a vector encoding untagged β_3 or β_1 integrin to ensure proper localization of the integrin $\alpha\beta$ heterodimer (some PA-FP integrin α_v localizes to endoplasmic reticulum without β co-expression). The untagged β_3 and β_1 integrins were gifts from Dr. Mark Ginsberg, UCSD School of Medicine. High level of talin-head expression appeared to affect cell spreading and the cells were transfected at 1:20 dilution relative to manufacturer's protocol.

Supplementary Note 4

Characterization of PA-FP Fusion Protein Expression Level

To quantify the expression levels and the molecular weight of the PA-FP constructs relative to endogenous expression levels, western blotting of transfected cells lysates was carried out. Transfected cells were plated in 10 cm tissue culture dishes, and harvested after 1 day in culture (37° C, 5 % CO₂). Cells were collected in lysis buffer (50 mM tris pH 8.0, 150 mM NaCl, 5 mM EDTA, 5% Glycerol, 1% Triton X-100) supplemented with protease inhibitor cocktail (Roche). Cells were freeze-thawed 3 times in liquid nitrogen and clarified by centrifugation at 16,000 g for 20 minutes at 4° C. Lysates with 10 µg of total protein were run on 4-12 % gradient PAGE gels. FA proteins were then probed by antibodies as described previously³⁸. The expressed proteins were observed at increased molecular weight as expected from the fused PA-FP (data not shown). From the intensity ratio between the endogenous and PA-FP fusion protein bands, the amount of plasmid DNA required to obtain PA-FP fusion expression level of that is less than endogenous level were determined (typically ~ 1 µg of vector except for FAK, 0.4 µg, VASP, 0.1 µg and α -actinin 0.1 µg, per 10⁶ cells) for the transfection of cells for iPALM imaging.

Co-Immunoprecipitation of Talin Fusion Constructs and Endogenous Talin

Since talin is believed to form a homodimer via C-terminal interactions²⁶, we were concerned whether the Talin-C construct having the FP near the reported dimerization sequence may affect this capability. Therefore, we tested whether both talin-N and talin-C constructs could dimerize properly with endogenous untagged talin. In Supplementary fig. 20, co-immunoprecipitation (IP) results show that both Talin-N and Talin-C can bind to and co-precipitate endogenous talin and vice versa. Together with their proper localization in FAs (Supplementary fig. 5) and previous characterization of Talin-N³⁹, this suggests that our talin fusion proteins should properly report the localization and orientation of endogenous talin in cells.

U2OS (human osteosarcoma) cells (8 x 10⁶ cells) were transfected with plasmids encoding Talin-N or Talin-C fusion proteins using Amaxa® transfection system (Lonza). We used the GFP-based constructs instead of tdEos since anti-GFP antibody is available (EGFP-18-talin1 for Talin-N and talin1-22-mEmerald for Talin-C). For control, non-transfected cells (Mock), and cells transfected with pmaxGFP vector (DNC-0053-15, control vector supplied with Amaxa kit) were used. After transfection, cells were plated in 10 cm tissue culture dishes, and harvested after 1 day in culture (37° C, 5 % CO₂). Cells were collected in lysis buffer (50 mM

tris pH 8.0, 150 mM NaCl, 5 mM EDTA, 5% Glycerol, 1% Triton X-100) supplemented with protease inhibitors cocktail (Roche). Cells were freeze-thawed 3 times in liquid nitrogen and clarified by centrifugation at 16,000 g for 20 minutes at 4° C. Lysates were then precleared for 1 h at 4° C with anti-mouse IgG or anti-rabbit IgG beads. For immunoprecipitation of endogenous talin, 800 µg of total proteins were used, while 500 µg total proteins were used for immunoprecipitation of expressed talin constructs. The lysates were incubated with 1 µg of anti-human talin antibody which does not recognize the mouse talin of the Talin-N or Talin-C constructs (clone 1676, Chemicon International) or 1 µg anti-GFP (Abcam) over night at 4° C. The following day, 30 µl protein IgG beads were added and the samples incubated in a rotator at 4°C for 1 h. Beads were then washed 3 times with lysis buffer and resuspended in 30 µl 2x Laemmly sample buffer. Samples were then analyzed by Western blotting using 4-12% gradient polyacrylamide gels (Invitrogen, Carlsbad, CA).

Supplementary Note 5

Rationale and considerations in the application of superresolution microscopy to study Focal Adhesions (FA)

The development of superresolution microscopy is motivated by a common aim of addressing the limitations of conventional light and electron microscopy methods. We refer readers interested in the physical principles, historical perspectives, as well as practical applications of superresolution light microscopy to reviews such as Ref. 17 and ⁴⁰⁻⁴⁴, where in-depth considerations regarding their strengths, limitations, and suitability for a wide range of biological applications are also discussed. In this study, we made use of iPALM 3D superresolution technique, whose theoretical foundation, experimental characterization, and validation have been described earlier⁹. We note that iPALM is one of many emerging techniques of superresolution microscopy which continues to advance rapidly and that these methods typically have many common capabilities, and thus several may be suitable for a given biological system. In the following, we discuss important considerations and technical details with particular attention to the study of focal adhesions (FAs).

Since the size scale of FAs is <200-nm vertically^{5,6}, high effective 3D spatial resolution, approaching the size scale of the protein components, is important. In particular, such relatively compact vertical (z) dimension of the structure suggests opposing-lens based method (4π geometry⁴⁵) such as iPALM⁹, iSMS⁴⁶, i5M⁴⁷, or isoSTED⁴⁸ may be advantageous compared to single lens approaches¹⁷. For highly dense protein structures such as FAs, high effective spatial resolution depends on a combination of both high density labeling of the structure of interest to satisfy the Nyquist-Shannon sampling theorem⁴⁹ and the high effective resolution of the imaging method. Due to the typically sparse targeting to structures of interest by immuno-metal probes⁶, the former requirement has long been a main limitation for electron microscopy (EM) of FA proteins. This is addressed by fluorescence-based super-resolution imaging using high density and high molecular specificity labeling strategies, such as fluorophore-conjugated antibodies or genetically encoded fluorescent proteins⁴⁴. For the latter requirement, optimal resolution depends not only on the optical configuration but also on the fact that at sufficiently high resolution, the dimension of the imaging probe relative to the target becomes significant and could become the effective limit on the resolution. For example, since an IgG antibody molecule is ~15 nm long, using primary and secondary antibodies for labeling introduces significant additional uncertainty, as shown by microtubule imaging with anti-tubulin antibodies where ~60 nm diameter is reported^{50,51}, whereas the actual diameter of microtubule is ~25 nm. Thus, in such cases the brightness advantage of synthetic fluorophores, which can be localized

to higher accuracy due to higher brightness³³, is offset by the labeling approach. Several approaches for labeling proteins with bright synthetic fluorophores with small effective tag size are discussed in Ref.⁴⁴. Additionally, multi-color imaging⁴⁸ or further deconvolution analysis⁵² has also been demonstrated to significantly enhance the capability of existing techniques and should be explored further. For our FA application, we make use of photoactivatable fluorescent proteins (PA-FP), which combine relatively small probe size at ~4 nm across and sufficient brightness for localization-based imaging methods, as demonstrated by the resolution of PA-FP labeled microtubule diameter to 25-30 nm by iPALM⁹. The FA system is also particularly amenable to iPALM analysis since their compact vertical dimensions are well within the size of an interference fringe, and thus potential complications from vertical coordinate periodicity resulting from interferometry can be straightforwardly minimized by using total internal reflection illumination condition for excitation⁹.

Supplementary Note 6

References cited in Online Methods and Supplementary Notes

- 31 E. Dulkeith et al., Plasmon emission in photoexcited gold nanoparticles, *Physical Review B* **70** (20), 205424 (2004).
- 32 W. H. Press, P. P. Flannery, S. A. Teukolsky, and W. T. Vetterling, *Numerical recipes*. (Cambridge Univ. Pr., 1986).
- 33 R. E. Thompson, D. R. Larson, and W. W. Webb, Precise nanometer localization analysis for individual fluorescent probes, *Biophys J* **82** (5), 2775 (2002).
- 34 J. E. Aubin, Autofluorescence of viable cultured mammalian cells, *J Histochem Cytochem* **27** (1), 36 (1979).
- 35 E. Zamir et al., Molecular diversity of cell-matrix adhesions, *J Cell Sci* **112** (Pt 11), 1655 (1999).
- 36 Neyfakh, A.A., Jr., Tint, I.S., Svitkina, T.M., Bershadsky, A.D., & Gelfand, V.I., Visualization of cellular focal contacts using a monoclonal antibody to 80 kD serum protein adsorbed on the substratum. *Experimental cell research* **149** (2), 387-396 (1983).
- 37 Tumbarello, D.A., Brown, M.C., Hetey, S.E., & Turner, C.E., Regulation of paxillin family members during epithelial-mesenchymal transformation: a putative role for paxillin delta. *J Cell Sci* **118** (Pt 20), 4849-4863 (2005).
- 38 Pasapera, A.M., Schneider, I.C., Rericha, E., Schlaepfer, D.D., & Waterman, C.M., Myosin II activity regulates vinculin recruitment to focal adhesions through FAK-mediated paxillin phosphorylation. *J Cell Biol* **188** (6), 877-890.
- 39 Franco, S.J. et al., Calpain-mediated proteolysis of talin regulates adhesion dynamics. *Nat Cell Biol* **6** (10), 977-983 (2004).
- 40 Bewersdorf, J., Schmidt, R., & Hell, S.W., Comparison of I5M and 4Pi-microscopy. *J Microscopy* **222** (Pt 2), 105-117 (2006).
- 41 Patterson, G., Davidson, M., Manley, S., & Lippincott-Schwartz, J., Superresolution imaging using single-molecule localization. *Ann Rev Phys Chem* **61**, 345-367 (2010).
- 42 Huang, B., Bates, M., & Zhuang, X., Super-resolution fluorescence microscopy. *Ann Rev Biochem* **78**, 993-1016 (2009).
- 43 Heintzmann, R. & Gustafsson, M.G.L., Subdiffraction resolution in continuous samples. *Na Photonics* **3** (7), 362-364 (2009).
- 44 Fernández-Suárez, M. & Ting, A.Y., Fluorescent probes for super-resolution imaging in living cells. *Nat Rev Mol Cell Biol* **9** (12), 929-943 (2008).
- 45 Hell, S. & Stelzer, E.H.K., Properties of a 4Pi confocal fluorescence microscope. *J Opt Soc America A* **9** (12), 2159-2166 (1992).
- 46 Middendorff, C., Egner, A., Geisler, C., Hell, S.W., & Schönle, A., Isotropic 3D Nanoscopy based on single emitter switching. *Optics Express* **16** (25), 20774-20788 (2008).
- 47 Gustafsson, M.G.L., Agard, D.A., & Sedat, J.W., Sevenfold improvement of axial resolution in 3D widefield microscopy using two objective lenses. *Proc. SPIE*, **2412**, 147-156 (1995).
- 48 Schmidt, R. et al., Spherical nanosized focal spot unravels the interior of cells. *Nat Methods* **5** (6), 539-544 (2008).
- 49 Shroff, H., Galbraith, C.G., Galbraith, J.A., & Betzig, E., Live-cell photoactivated localization microscopy of nanoscale adhesion dynamics. *Nat Methods* **5** (5), 417-423 (2008).
- 50 Huang, B., Wang, W., Bates, M., & Zhuang, X., Three-dimensional super-resolution imaging by stochastic optical reconstruction microscopy. *Science* **319** (5864), 810-813 (2008).

- 51 Bates, M., Huang, B., Dempsey, G.T., & Zhuang, X., Multicolor super-resolution imaging
with photo-switchable fluorescent probes. *Science* **317** (5845), 1749-1753 (2007).
- 52 Egner, A., Jakobs, S., & Hell, S.W., Fast 100-nm resolution three-dimensional
microscope reveals structural plasticity of mitochondria in live yeast. *Proc Natl Acad Sci
USA* **99** (6), 3370 (2002).